Dept. of Communications Engineering

Orbit Simulation Satellite Formation Flights in LEO

Project Thesis

submitted by

Zhengyu Chen

Bremen, October 30, 2022

Universität Bremen

Orbit Simulation Satellite Formation Flights in LEO

Fachbereich 1 - Physics and Electronical Engineering
Institute for Telecommunications and High-Frequency Techniques (ITH)
Department of Communications Engineering
P.O. Box 33 04 40
D-28334 Bremen

Supervisor:	Shengdi Wang, Maik Röper
First Examiner:	Prof. Dr.-Ing. Armin. Dekorsy

I ensure the fact that this thesis has been independently written and no other sources or aids, other than mentioned, have been used.

Bremen, October 30, 2022

. . . . . .

Contents

Chapter 1

Introduction

In the current satellite systems, it is often advantageous to make use of several micro-satellites to allow satellites which fly in a formation to perform different missions like remote sensing, satellite communication and GPS services for terrestrial application scenarios. Because they are cheaper and easier to manufacture compare with large sophisticated satellite. Thus in this thesis, we firstly investigate the classic satellite motion that only experience gravitational force and satellite formation strategy in Low Earth Orbit (LEO), which means satellite orbital height is smaller than 2000km. The reason of choosing low earth orbit is to spend smallest amount of energy to place satellite in outer space and therefore satellites could reduce the burden on building powerful amplifier for data transmission.

To solve unperturbed satellite motion, the two-body problem [8] needs to be solved that can explain shape of satellite trajectory based on eccentricity. Subsequently, Orbital elements are introduced to precisely define satellite orientation. Also, to simulate satellite motion and visualize satellite projection on the Earth's surface according to these theoretical foundations, we come to Earth-centered Inertial (ECI) frame and Earth-centered,Earth-fixed (ECEF) frame and the transformation in between. However, to investigate inter-satellite satellite relative motion and how they achieve formation flying, the Local-Vertical-Local-Horizontal (LVLH) frame with incorporation of the Hill-Clohessy-Wiltshire (HCW) equations [0] which offers a linearized dynamic model to describe one satellite relative motion in a satellite-oriented frame is applied. To achieve bounded satellite formation flying which different satellites move in a finite distance range with respect to each other, specific initialization of satellite in LVLH frame is chosen to generate the Projected Circular Orbit (PCO) and General Circular Orbit (GCO) [0]. Additionally, we extend conception of PCO to the triangular satellite formation that could be used in remote sensing imaging etc.

Thomas Carter and Mayer Humi provided a simplified drag-modified HCW model to incorporate quadratic atmospheric drag force into satellite relative motion [6]. Also, the J2 modified HCW equations are introduced to deal with effect of inhomogeneous distribution of Earth gravitational field to classic HCW model. Thus, their effects are studied

and compared from a deputy-chief satellite formation with PCO at low orbital height.

Ultimately, the Kalman Filter (KF) and Extended Kalman Filter (EKF) are applied for position and velocity estimation of deputy satellite in LVLH frame at time step k based on these models with the measurements from sensors and position and velocity estimate at step $k-1$. The sensors measure the distance and velocity of deputy satellite with respect to chief satellite in chief-oriented LVLH frame. Further estimation analysis include process and observation noise effects to their performance and convergence are done to choose noise levels that achieve different tracking accuracy.

Chapter 2

The Satellite Orbital Mechanics

In modern space missions like orbit maneuver, space rendezvous and interplanetary orbit transfer, it is necessary to precisely know the motion pattern of these space shuttles. Therefore, the satellite orbital mechanics provides a solid theoretical foundation to describe satellite's motion and then different control mechanisms can be applied to achieve different space missions. As a rule of thumb, the two-body problem in this chapter illustrates the unperturbed motion of satellite. In addition, perturbations are needed to be implemented into their unperturbed motion pattern to have a more precise motion description in real space environment. In this chapter, we investigate J2 perturbation and atmospheric drag force, which are two major perturbations that influence satellite in Low Earth Orbit to achieve this goal.

2.1 Two-body Problem

The motion trajectory of satellite is essential to astronomy and aeronautics to offer a clue how to locate satellite position and further manipulate and optimize its trajectory to fulfill different space missions. Basically, satellite motion could be spilt into two parts: unperturbed motion under purely gravitational force and perturbed motion with the presence of, e.g., atmospheric drag force [1] and earth flattening effect [1] etc. In this section, the physics behind satellite motion under gravitational force is discussed.

Firstly, a two-body problem shown in Fig 2.1 is came up with: how these two bodies will move under interaction of gravitational force with each other? Here body 1 are 2 are earth and satellite and assume they have weight as m_1 and m_2. The gravitational force acting on body 1 by body 2 and on body 2 by body 1 can be written as:

$$\mathbf{F}_{12} = m_1 \frac{\mathrm{d}^2 \mathbf{r}_1}{\mathrm{d}t^2} \tag{2.1}$$

$$\mathbf{F}_{21} = m_2 \frac{\mathrm{d}^2 \mathbf{r}_2}{\mathrm{d}t^2} \tag{2.2}$$

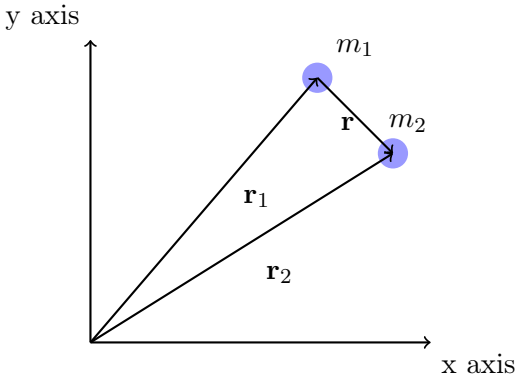

Figure 2.1: Two Body Problem

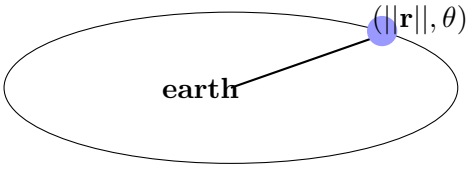

Figure 2.2: One Body Problem

Then divide by m_1 and m_2 on both sides of (2.1) and (2.2), after some manipulations [8], gravitational force experienced by satellite can be obtained as:

$$\mathbf{F_{12}} = m_r \frac{\mathrm{d}^2\mathbf{r}}{\mathrm{d}t^2} \tag{2.3}$$

here $m_r = \frac{m_1 m_2}{m_2 + m_1}$ and is called reduced mass. From observation of this equation, a conclusion can be drawn as movement of satellite under earth gravitational force is equivalent as a body with reduced mass m_r moves under gravitational force pointing to direction of $\mathbf{F}_{12}$. Then the original two-body problem has been reduced as one-body problem shown in Fig 2.2 and it is convenient to use polar coordinate $\mathbf{r} = (||\mathbf{r}||, \theta)$ to indicate satellite position vector $\mathbf{r}$. From system point of view, earth and satellite forms a basic system and its total energy E_e must be conserved as shown below if there is no external force.

$$E_e = \frac{1}{2} m_r ||\mathbf{v}||^2 - \frac{G m_1 m_2}{||\mathbf{r}||^2} \tag{2.4}$$

where G is gravitational constant and equal to 6.67408e-11 $\mathrm{m^3 kg^{-1} s^{-2}}$ and $\mathbf{v}$ is velocity vector of satellite. Meanwhile velocity vector can be spilt into radial direction and tangential direction as:

$$\mathbf{v} = \frac{d\mathbf{r}}{dt} + \mathbf{r}\frac{d\theta}{dt} \tag{2.5}$$

By substitute this velocity expression in (2.4) and solve it, we could rewrite it as a formula that describes satellite position vector magnitude $||\mathbf{r}||$ in relation to a parameter called eccentricity (e) and polar angle θ is given in (2.6), the detailed derivation can be seen in reference [8]:

$$||\mathbf{r}|| = \frac{r_0}{1 - ecos(\theta)} \tag{2.6}$$

where $r_0 = \frac{||\mathbf{h}||^2}{Gm_r m_1 m_2}$ depends on angular momentum of satellite $\mathbf{h} = \mathbf{r} \times \mathbf{v}$. This equation implies that bounded satellite trajectory under attractive gravitational force will be an ellipse or circle, depends on eccentricity e, which is a theoretical foundation of orbital elements illustration in further sections. Interestingly, for an initial circular orbit, orbital equation in (2.6) can be reduced with the equivalence between centrifugal acceleration and gravity acceleration as:

$$\frac{||\mathbf{v}||^2}{||\mathbf{r}||} = \frac{GM}{||\mathbf{r}||^2} \tag{2.7}$$

where GM is standard gravitational parameter and equals to 398.6004e12 $\mathrm{m^3 s^{-2}}$. Then, after rearrangement, the proper velocity and position magnitude $||\mathbf{r}||$ and $||\mathbf{v}||$ of satellite need to be chosen to fulfill condition in (2.7) and generate a circular orbit with angular momentum magnitude $||\mathbf{h}||$ as [1]:

$$||\mathbf{r}|| = \frac{||\mathbf{h}||^2}{GM} \tag{2.8}$$

2.2 Orbital Elements

From prior knowledge of circular or elliptical shape of satellite trajectory the unique position of satellite at a specific time step on the specific orbit could be determined with the conceptions of orbital elements, which consists of six physical quantities shown in Fig 2.3. Their derivation could be found in [1].
Here the perturbations that acting on the satellites are out of consideration and thus we only consider the gravitational force that they are experiencing for calculations. All these elements are shown in Fig 2.3.

Semi-major Axis (a) is defined as the distance between the satellite elliptical orbit center which is also the Earth center and perigee point shown in the Fig 2.3, which can be calculated as [1]:

$$a = \frac{1}{\frac{2}{||\mathbf{r}||} - \frac{||\mathbf{v}||^2}{GM}} \tag{2.9}$$

The **Eccentricity** (e) is a parameter ranges from 0 to infinity and used to describe the

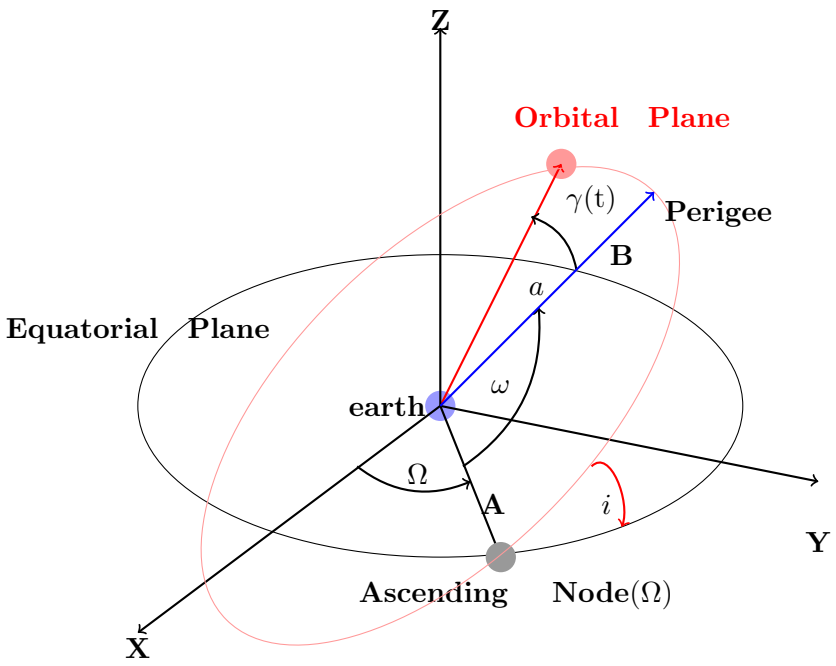

Figure 2.3: Orbital Elements Illustration

shape of satellite's orbit trajectory [1]. For elliptical orbit we have $0 < e < 1$ and for circular orbit we have $e = 0$.

$$e = \sqrt{1 - \frac{||\mathbf{h}||^2}{GMa}} \tag{2.10}$$

The Longitude of Ascending Node (Ω) is the angular distance from the intersection of orbital plane and equatorial plane noted as black dot in Fig 2.3 to the vernal equinox axis (x-axis), in order to calculate it, we introduce the node vector $\mathbf{A} = \mathbf{Z} \times \mathbf{h}$ and $\mathbf{Z} = [0 \quad 0 \quad 1]^T$. This vector is pointing towards Ascending node which is denoted as A in Fig 2.3 and therefore Ascending node angle is the angle between node vector $\mathbf{A}$ and its component in X-axis direction $\mathbf{A_x}$ then we can directly calculate Ascending node as :

$$\Omega = \arccos\left(\frac{||\mathbf{A_x}||}{||\mathbf{A}||}\right) \tag{2.11}$$

The Inclination Angle (i) is the angular difference between equatorial plane and orbital plane and therefore it is angle of angular momentum vector $\mathbf{h}$ and $\mathbf{Z}$, which is the unit vector of Z-axis in Fig 3.3, then we take the dot product of these two vectors to calculate it:

$$i = \arccos\left(\frac{\mathbf{h}\cdot\mathbf{Z}}{||\mathbf{h}||}\right) \tag{2.12}$$

The Argument of Perigee (ω), which is the angular distance between Ascending Node and Perigee in Fig 2.3. Then its just the angle between the perigee vector which is denoted as **B** in Fig 2.3 and ascending node vector **A**:

$$\omega = \arccos\left(\frac{\mathbf{A}\cdot\mathbf{B}}{||\mathbf{A}||||\mathbf{B}||}\right) \tag{2.13}$$

Meanwhile, perigee vector **B** can be calculated with assistance of satellite position and velocity vector **r** and **v** as [1]:

$$\mathbf{B} = \frac{1}{GM}((||\mathbf{v}||^2 - \frac{G}{r})\mathbf{r} - (\mathbf{r}\cdot\mathbf{v})\mathbf{v}) \tag{2.14}$$

True Anomaly (γ(t)) is the angle between satellite radius vector that is shown as red line with arrow in Fig 2.3 and perigee vector **B** shown as blue line with arrow in Fig 2.3. True anomaly is changing with time for a given unperturbed satellite orbit, whereas other five elements are fixed, and it can be calculated as:

$$\gamma(t) = \arctan\left(\sqrt{\frac{1-e}{1+e}}tan(\frac{q}{2})\right) \tag{2.15}$$

where q is eccentric anomaly and shown in the Fig 2.4, which is the angular distance from satellite and denoted as red circle in Fig 2.4 and earth denoted as gray circle in Fig 2.4, in an origin-oriented frame. With geometric relation we have:

$$||\mathbf{r}|| = a(1 - e\cos q) \tag{2.16}$$

After rearrangement, we get:

$$q = \arccos\left(\frac{1}{e}(1 - \frac{||\mathbf{r}||}{a})\right) \tag{2.17}$$

Additionally, the mean anomaly can also be regarded as substitution of sixth orbital element, which is defined as the angular distance that satellite would have, if it which is shown as blue circle in Fig 2.4 is moving in an assumed circular orbit with a constant angular velocity and same orbital period in the real satellite elliptical orbit as shown in Fig 2.4. It can be calculated as:

$$M = n(t - t_0) \tag{2.18}$$

where n is angular velocity of satellite in the visualized circular orbit and t_0 is initial time point for calculation. It is quite often used in satellite geodesy to specify satellite position,

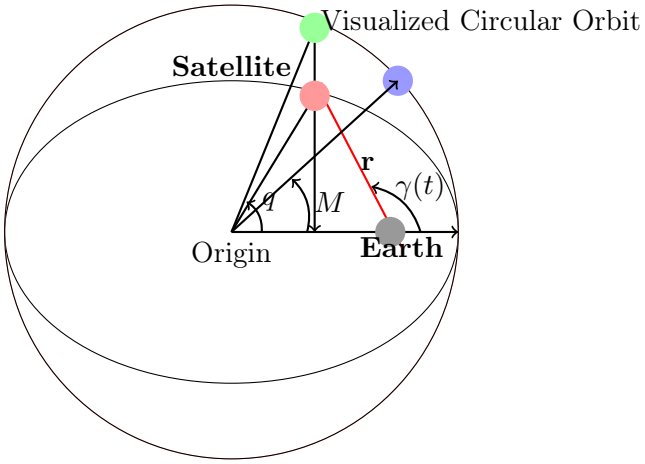

Figure 2.4: Eccentric, Mean and True Anomaly Illustration

since it can be interpolated with time [1]. Then we introduce the Kepler equation that given the relation between mean anomaly, eccentricity and eccentric anomaly as below:

$$M = q - esin(q) \tag{2.19}$$

2.3 Perturbed Satellite Mechanics

The two most important perturbations influence satellite position in Low Earth Orbit are J2 perturbation and atmospheric drag force and also need to be implemented in HCW model for real scenario in space missions.

2.3.1 J2 Perturbation

In previous satellite motion demonstrations, the earth flattening effect is not taken consideration. However, earth is not a perfect spherical body but an ellipsoid, thus it causes inhomogeneous gravitational field distribution and acting significantly on satellite in the low earth orbit. This effect will drift ascending node of satellite orbit and trying to rotate satellite orbit and also cause variations in all other orbital elements. The gravitational filed distribution related to geocentric latitude ϕ is given as follows [1]:

$$V = -\frac{GM}{||\mathbf{r}||}(1 - \sum_{b=2}^{\infty} J_b(\frac{a_e}{||\mathbf{r}||})^b P_b(\sin(\phi))) \tag{2.20}$$

- a_e the mean earth radius and equal to around 6.7318e6 m

- $P_b(\sin(\phi))$ The Legendre polynomial with order b

J_b is spherical harmonic coefficient with order b. Only consider $J_2 = 1.083e-3$, since it is 1000 times larger than higher order terms like J_3. Also, if we only consider J2 term, (2.20) can be written as the combination of unperturbed gravitational potential V_u resulting from uniformly distributed earth gravitational field and disturbing potential V_{j2}.

$$V = \underbrace{-\frac{GM}{||\mathbf{r}||}}_{V_u} + V_{j2} \tag{2.21}$$

The J2 perturbation decays significantly with increasing orbital height $||\mathbf{r}_o||$ due to $(\frac{1}{||\mathbf{r}||^3})$ term that can be seen from (2.20). This can be seen the disturbing potential energy variation caused by J2 effect with different orbital heights in table 2.1. The orbital height $||\mathbf{r}_o||$ is calculated as:

$$||\mathbf{r}_o|| = ||\mathbf{r}|| - a_e \tag{2.22}$$

$\|\|\mathbf{r}_o\|\|$(km)	V_{j2}(J)
40.186	29389.66
50.186	28126.67
60.186	26935.02

Table 2.1: Disturbing Potential with J2 Effect on Different Orbital Height

2.3.2 Atmospheric drag force

The atmospheric drag force is caused by atmospheric disturbance for LEO and acting to pull the satellite closer to earth surface, which has an anti-parallel direction with respect to satellite velocity direction. The acceleration caused by this force is:

$$\mathbf{a}_{drag} = -\frac{\rho C_0 A}{2m}||\mathbf{v}||\mathbf{v} \tag{2.23}$$

- ρ atmospheric density
- C_0 drag coefficient, dimensionless which depends majorly on the shape of satellite.
- A Satellite cross-sectional area which is perpendicular to its moving direction
- m Satellite mass

The atmospheric density at given orbital height $||\mathbf{r}_o||$ is given as barometric formula:

$$\rho = \exp\left(\frac{-||\mathbf{r}_o||}{H}\right) \tag{2.24}$$

, where H is scale height and equal to 8.5e3 for a given air temperature T of 290K. The scale height corresponds to an increment of altitude which cause atmospheric pressure decreases by the factor of the base of natural logarithmic e, roughly 2.718. It can be calculated as:

$$H = \frac{k_e T}{mg} \tag{2.25}$$

,where $k_e = 1.38e - 23$ JK^{-1} and it's Boltzmann constant, g is gravitational acceleration and equal to 9.81 m/s^2. Therefore, from barometric formula we can observe atmospheric density decreasing exponentially with increasing altitude and thus drag perturbation only usually dominate in the low earth orbit with orbital height smaller than 50 km and could be neglected beyond this orbital height range.

Chapter 3

Satellite Motion in Different Frames and Formation Flying

In space missions, the orientation of satellites must be precisely defined and therefore different coordinate systems are came up with to provide a mathematical representation of satellite location in space. In this chapter, three different frames are introduced for different purposes: ECI frame, ECEF frame and LVLH frame.

3.1 ECI Coordinate System

The ECI coordinate system is commonly used to describe satellite motion in a very convenient way. In this coordinate system, we don't consider the rotation of earth with respect to sun and it's a non-rotating frame, while earth will keep its self-rotation. Also, we set the earth's center as the origin in the coordinate system. The x-y plane of ECI frame is overlapped with equatorial plane, while z axis will extend to the North Pole of Earth. Therefore, it enables us to represent the motion equation of satellite simpler in ECI frame.
The state of satellite consist of its position and velocity vector at a specific time point in the chosen frame, which explains its motion characteristic at this time point. For a given satellite state, we would have its velocity vector $\mathbf{v} = [v_x \quad v_y \quad v_z]^T$and also the position vector $\mathbf{r} = [r_x \quad r_y \quad y_z]^T$ under the Cartesian ECI coordinate system. On the basis of 6 orbital elements, we can calculate the Cartesian coordinates in ECI frame in spherical coordinate representation:

$$\mathbf{r} = \begin{bmatrix} r_x \\ r_y \\ r_z \end{bmatrix} = \begin{bmatrix} ||\mathbf{r}||(\cos(\omega + \gamma(t))\cos(\Omega) - \sin(\omega + \gamma(t))\sin(\omega)cos(i)) \\ ||\mathbf{r}||(\cos(\omega + \gamma(t))\sin(\Omega) - \sin(\omega + \gamma(t))cos(\omega)cos(i)) \\ ||\mathbf{r}||(\sin(i)\sin(\omega + \gamma(t))) \end{bmatrix} \tag{3.1}$$

With a given initial satellite state in ECI frame, in spite of true anomaly $\gamma(t)$, other 5 orbital elements can be determined and are fixed during orbital revolution. As we can see that true anomaly is time-varying and its calculus needs the knowledge of eccentric anomaly from (2.15). For numerical implementation of satellite coordinates in ECI frmae, firstly we could calculate true anomaly from eccentric anomaly as the approximation done by the Newton Method [2] with updating mean anomaly M in a given satellite orbital period T.
With Kepler third Law, the orbital period is calculated with Semi-major axis (a) and gravitational constant GM:

$$T = 2\pi\sqrt{\frac{a^3}{GM}} \tag{3.2}$$

Recall Kepler equation in (2.19) to calculate eccentric anomaly q. Then we can construct a function that:

$$f(x) = M - q + esin(q) \tag{3.3}$$

, then we find q corresponds to zeros of (3.3) and thus Newton method that calculates zeros of a function $f(x)$ based on function itself and its first order derivative could be applied, we could calculate eccentric anomaly at a given time point via this iterative numerical approximation:

$$q_{i+1} = q_i - \frac{f(q_i)}{\dot{f}(q_i)} \tag{3.4}$$

For mean anomaly at a given point, we could replace it as:

$$M = q_i \tag{3.5}$$

, then insert $f(q_i)$ and $\dot{f}(q_i)$ and we could calculate eccentric anomaly at this point via iteration as follows:

$$q_{i+1} = q_i - \frac{q_i - esin(q_i) - M}{1 - ecos(q_i)} \tag{3.6}$$

In general, this iteration is usually taken for several times to improve accuracy. Also, mean anomaly is updated in one orbital period with a given angular velocity from (2.18). Ultimately, we could update true anomaly over satellite orbital revolution via calculus of eccentric anomaly q with updating known mean anomaly M in (3.5)-(3.6), then Cartesian coordinates of Satellite in ECI frame could be solved with (3.1).

Then the motion of 4 micro-satellites in low earth orbit is simulated in Fig 3.1, the initial parameters are set in Table 3.1. To investigate how velocity magnitude of satellite changes orbital shape and causes different variations in orbital height, these four satellite are launched at same position for convenience ($\mathbf{r} = [-6800km, 0km, 0km]$). The velocity vector magnitude are chosen differently but with same direction to study how velocity magnitude of satellite affects orbital height as in table 3.1:

	Ω(in Radians)	e	||v||(m/s)	i(in Radians)	ω	a(km)
Satellite 1	0	0.0379	7800	0.6403	2.3562	7068
Satellite 2	0	0.0573	7850	0.7450	2.3562	7167.4
Satellite 3	0	0.0647	7900	2.5013	2.3562	7270.4
Satellite 4	0	0.0782	7950	1.9756	2.3562	7377

Table 3.1: Satellite Network Parameter Setting in LEO

The orbital height profile of all four individual satellites have a sinsuidal shape and also satellite with larger velocity will have a larger semi-major axis according to (2.9) and will overcome earth gravitational effect and show smaller variation in orbital height as shown in Fig 3.1. The orbital simulation scenario of four satellites are shown in Fig 3.2.

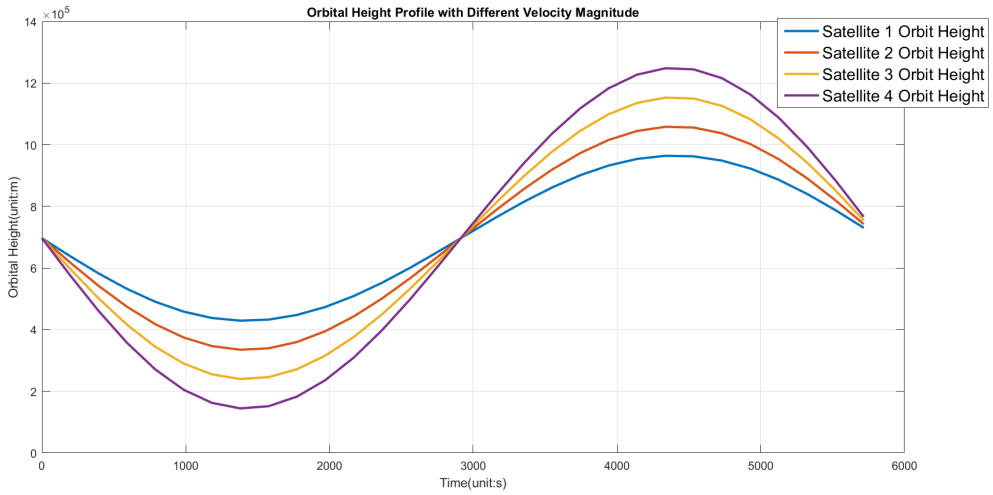

Figure 3.1: Satellite Orbit Height Comparison

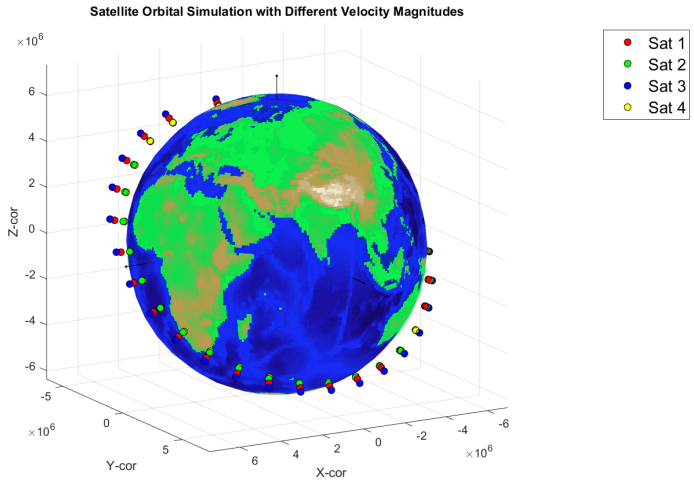

Figure 3.2: Orbital Simulation for Different Satellite Velocity Magnitudes

The maximum and minimum of orbital height correspond to the perigee and apogee in orbital plane. As seen in Fig 3.1, the variation of orbital height becomes smoother with decreasing velocity magnitude. Therefore, if we decrease velocity magnitude of satellite sufficiently, it means the orbital height profile will be a straight line which indicates a circular orbit. This means circular orbit possesses the minimum velocity magnitude of satellite among all kinds of satellite orbit shape.

3.2 The ECEF Coordinate System

In this part, the ECEF coordinate system is used to determine the satellite orbit position on the earth surface in an easier way and then we could have a precise knowledge of satellite geological location . The difference between ECEF coordinate system and ECI coordinate system is that ECEF coordinate system is rotating with earth self-rotation rate, regardless of earth precession. Thus for the objects on the earth surface are fixed in ECEF coordinate system. This enables us to visualize satellite motion on earth surface by calculating the geodetic coordinate S= (ζ, λ) latitude λ and longitude ζ coordinate as below:

$$\zeta = \arctan\left(\frac{x_{ECEF}}{y_{ECEF}}\right) \tag{3.7}$$

$$\lambda = \arctan\left(\frac{z_{ECEF}}{\sqrt{x_{ECEF}^2 + y_{ECEF}^2 + z_{ECEF}^2}}\right) \tag{3.8}$$

Here $\mathbf{r}_{ECEF} = [x_{ECEF} \quad y_{ECEF} \quad z_{ECEF}]^T$, thus firstly it is necessary to transform ECI coordinates to ECEF coordinates to plot the projection of satellite motion in ECEF frame. The ECEF coordinate can be regarded as the rotated version of ECI cooridnates by the angle $w_{ie} \cdot t + G_m$ with z-axis, which is shown in Fig 3.3. The w_{ie} is earth rotation angular rate and is equal to $7.2921e-5/s$ and G_m is Greenwidch Mean sideral angle defined as hour angle at 0h which is the angle between dashed axis and ECI-X axis and thus rotated angle by ECEF system rotation is start from GMST, then we apply following rotational matrix to convert into ECEF coordinates [1]:

$$\begin{bmatrix} x_{ECEF} \\ y_{ECEF} \\ z_{ECEF} \end{bmatrix} = \begin{bmatrix} \cos(-G_m - w_{ie}t)) & \sin(-G_m - w_{ie}t) & 0 \\ -\sin(-G_m - w_{ie}t)) & \cos(-G_m - w_{ie}t) & 0 \\ 0 & 0 & 1 \end{bmatrix} \begin{bmatrix} x_{ECI} \\ y_{ECI} \\ z_{ECI} \end{bmatrix} \tag{3.9}$$

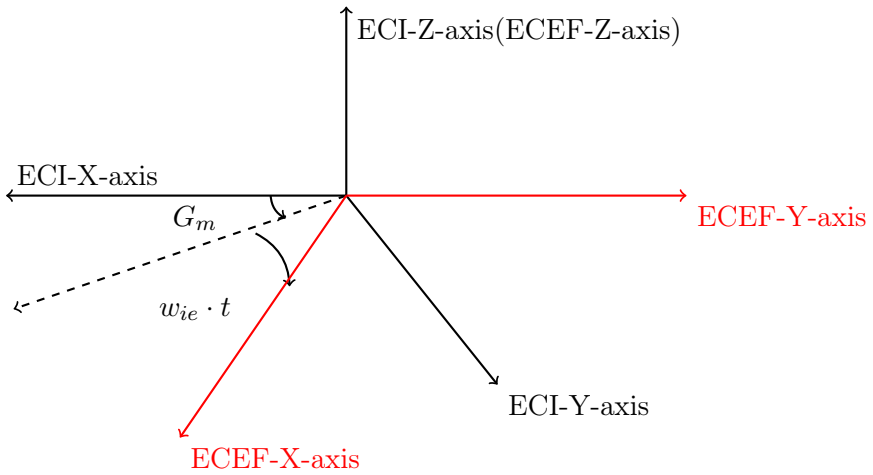

Figure 3.3: ECEF and ECI Coordinate system

The projection of satellite motion is plotted in Fig 3.4.

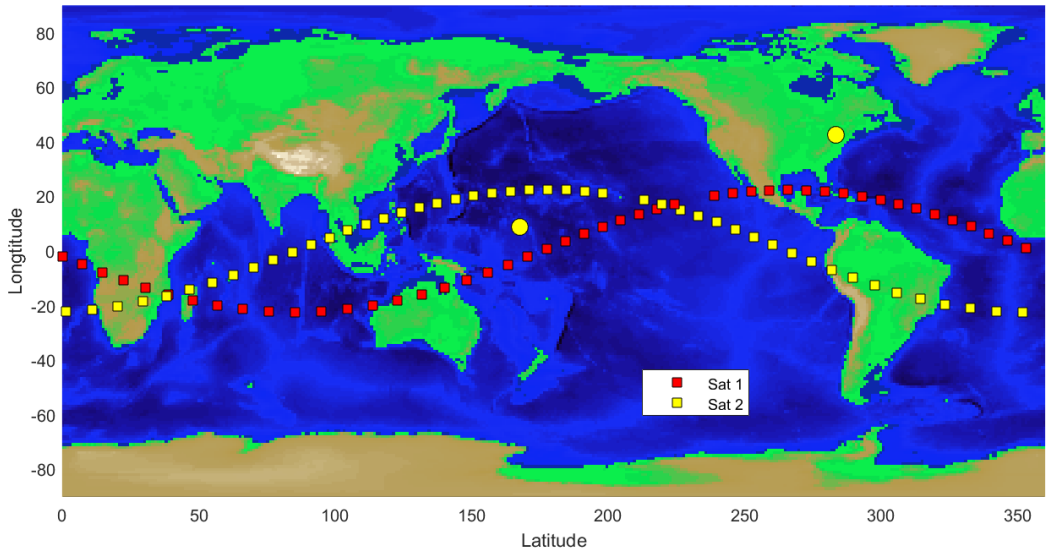

Figure 3.4: The Projection of Satellite Motion In ECEF Frame

3.2.1 The LVLH frame and HCW Equation

In order to precisely observe satellite motion investigate relative motion between satellites, it is often beneficial to scale the coordinate magnitude by using the LVLH frame. In this scenario, we set one satellite as origin in the LVLH frame and x axis refers to radial track direction and points at the radial direction of satellite, z-axis refers to cross-track direction which is perpendicular to the orbital plane and the y-axis refers to along-track direction and points at satellite velocity direction and completes the right-handed coordinate system . Thus coordinates of one satellite in a satellite-origin LVLH frame will be much smaller, instead of its ECI coordinates. The direction of three axis are shown as vector $\hat{\mathbf{i}}, \hat{\mathbf{j}}$ and $\hat{\mathbf{k}}$ in Fig 3.5. Consider a deputy-chief satellite scenario, to describe their relative motion in LVLH frame, we firstly come to their relative position vector in ECI frame $\mathbf{r}_{ECI}$:

$$\mathbf{r}_{ECI} = \mathbf{r}_d - \mathbf{r}_c \tag{3.10}$$

, where $\mathbf{r}_d$ and $\mathbf{r}_c$ are ECI position vector for deputy and chief satellite. In order to simulate both satellites motion in ECI frame under Keperian laws, it is neccessary to transform deputy satellite position vector in LVLH frame $\mathbf{r}_{LVLH}$ to its versions in ECI frame, then plus it with ECI state vector of chief satellite $\mathbf{r}_c$. To proceed it, it is reasonable to consider position vector in LVLH frame can be obtained, firstly rotate its version counterclockwisly in ECI frame ($\mathbf{r}_{ECI}$) about z-axis in ECI frame by angle Ω and then rotate it about x axis by angle of inclination (i). Then z-axis in ECI frame is aligned to z-axis in LVLH frame. Finally, the rotated vector should rotate counterclockwisly about z-axis by angle observed from argument of perigee ($w + \gamma(t)$) again to align x axis in ECI frame with respect to x-axis in LVLH frame in radial track direction.

$$\mathbf{r}_{LVLH} = \mathbf{R}_z(\Omega)\mathbf{R}_x(i)\mathbf{R}_z(w + \gamma(t))\mathbf{r}_{ECI} \tag{3.11}$$

, with following three rotation matrices [1]:

$$\mathbf{R}_z(w+\gamma(t)) = \begin{bmatrix} \cos(w+\gamma(t)) & -\sin(w+\gamma(t)) & 0 \\ \sin(w+\gamma(t)) & \cos(w+\gamma(t)) & 0 \\ 0 & 0 & 1 \end{bmatrix} \tag{3.12}$$

$$\mathbf{R}_x(i) = \begin{bmatrix} 1 & 0 & 0 \\ 0 & \cos(i) & -\sin(i) \\ 0 & \sin(i) & \cos(i) \end{bmatrix} \tag{3.13}$$

$$\mathbf{R}_z(\Omega) = \begin{bmatrix} \cos(\Omega) & -\sin(\Omega) & 0 \\ \sin(\Omega) & \cos(\Omega) & 0 \\ 0 & 0 & 1 \end{bmatrix} \tag{3.14}$$

Therefore, $\mathbf{r}_{ECI}$ can be derived as inverse transform with condition that all three rotation matrices have inverse, which means they are full rank and their determinant is nonzero:

$$\mathbf{r}_{ECI} = \mathbf{R}_z(w+\gamma(t))^{-1}\mathbf{R}_x(i)^{-1}\mathbf{R}_z(\Omega)^{-1}\mathbf{r}_{LVLH} \tag{3.15}$$

The HCW equation is used in this frame to describe the chief satellite relative motion with respect to a deputy satellite under following three assumptions:

- The initial distance between two satellites is very small compared to distance to earth center
- The chief satellite is moving on a circular orbit, while the deputy satellite moves in a circular or elliptical orbit
- The chief satellite moves with constant angular rate n.

Then we introduce the relative state in LVLH frame $\mathbf{x} = [\Delta x \quad \Delta y \quad \Delta z \quad \Delta\dot{x} \quad \Delta\dot{y} \quad \Delta\dot{z}]^T$, where $\Delta x, \Delta y, \Delta z$ are the LVLH coordinates in the direction of three axis shown in Fig 3.5 and $\Delta\dot{x}, \Delta\dot{y}, \Delta\dot{z}$ are velocity components in these three directions in LVLH frame. The HCW equation is a linearized version of relative motion that governs two satellites flying formation and given as following first order approximation as [0]:

$$\begin{aligned} \Delta\ddot{x} &= 3n^2\Delta x + 2n\Delta\dot{y} \\ \Delta\ddot{y} &= -2n\Delta\dot{x} \\ \Delta\ddot{z} &= -n^2\Delta z \end{aligned} \tag{3.16}$$

, where n is angular velocity of chief satellite that can be calculated as for an initial circular orbit with radius $||\mathbf{r}||$ for chief satellite [0]:

$$n = \sqrt{\frac{GM}{||\mathbf{r}||^3}} \tag{3.17}$$

These HCW second-order differential equations have an analytical solution of deputy satellite motion in x, y and z direction in LVLH frame as follows, the detailed derivation can be seen in appendix 7:

$$\Delta x(t) = A_x \cos(nt + \beta_x) + 4\Delta x_0 + \frac{2\Delta\dot{y_0}}{n} \tag{3.18}$$

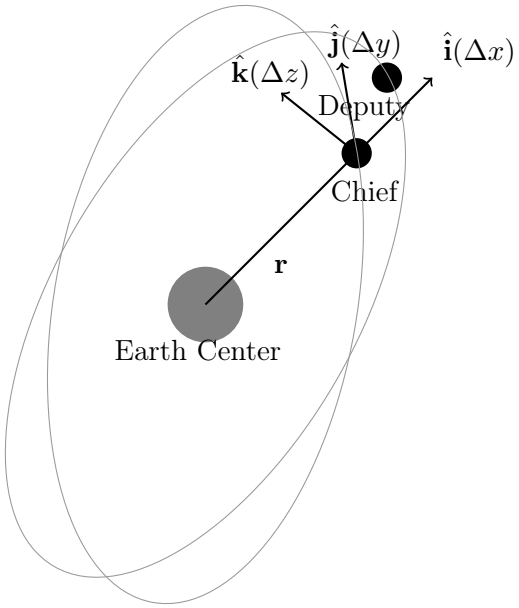

Figure 3.5: The Chief-Deputy Satellite Scenario in LVLH Frame

$$\Delta y(t) = -2A_x \sin(nt + \beta_x) + 2A_x \sin(\beta_x) + \Delta y_0 - 3(2n\Delta x_0 + \Delta \dot{y_0})t \tag{3.19}$$

$$\Delta z(t) = A_z \cos(nt + \beta_z) \tag{3.20}$$

The parameters A_x A_z β_x and β_z can be determined by initial state $\Delta\mathbf{x}_0 = [\Delta x_0, \Delta y_0, \Delta z_0, \Delta \dot{x_0}, \Delta \dot{y_0}, \Delta \dot{z_0}]$. Then equation 3.19 confirms relative motion of deputy satellite in y-direction of LVLH frame has an additional term $-3(2n\Delta x_0 + \Delta \dot{y_0})t$ that grows unboundedly with time t, which causes $|\Delta y(t)|$ increases continuously over time, while the displacements in x and z direction will vary in a finite range that constrained by cosine terms with a given $\Delta\mathbf{x}_0$ from 3.18 and 3.20. Therefore deputy satellite will gradually drift away with respect to chief satellite over time. Therefore the bounded relative trajectory can only be realized under the condition that this term is vanished. That implies:

$$2n\Delta x_0 + \Delta \dot{y_0} = 0 \tag{3.21}$$

Then a set of parameter solution that calculates parameters A_x A_z β_x and β_z with a known initial state can be given with constraint of 3.21 as:

$$A_x = \frac{\Delta x_0}{\cos(\beta_x)} \tag{3.22}$$

$$A_z = \frac{\Delta z_0}{\cos(\beta_z)} \tag{3.23}$$

$$\beta_x = \arctan\left(\frac{-\Delta \dot{x_0}}{n\Delta x_0}\right) \tag{3.24}$$

$$\beta_z = \arctan\left(\frac{-\Delta \dot{z_0}}{n\Delta z_0}\right) \tag{3.25}$$

3.2.2 PCO and GCO Formation Flying

To maintain a bounded satellite formation flying, an appropriate initial state set-up should be determined. In this section, we focus on two major Satellite formation strategies: PCO and GCO satellite formation. This difference between general circular orbit and projected circular orbit is the trajectory of deputy satellite in LVLH frame is a circle for general circular orbit, whereas it is an ellipse for projected circular orbit . The HCW equation solution for PCO is given in 3.27-3.29. The initial state $\Delta\mathbf{x}_0$ must fulfill 3.26 to make the trajectory projected onto y-z plane in LVLH frame is a circle:

$$A_z = -2A_x \tag{3.26}$$

$$\Delta x(t) = A_x \cos(nt + \beta_x) + 4\Delta x_0 + \frac{2\Delta\dot{y}_0}{n} \tag{3.27}$$

$$\Delta y(t) = -2A_x \sin(nt + \beta_x) + \Delta y_0 + 2A_x \sin(\beta_x) \tag{3.28}$$

$$\Delta z(t) = A_z \cos(nt + \beta_x) \tag{3.29}$$

For the GCO formation flying we have similar expression as (3.27)-(3.29) but only vary the parameters to fulfill condition:

$$A_z = -\sqrt{3}A_x \tag{3.30}$$

If we substitute (3.22) and (3.23) in (3.26) and let $\beta_x = \beta_z$, the constraints of $\Delta\mathbf{x}_0$ to get PCO formation flying can be obtained as (3.31)-(3.32):

$$-2\Delta x_0 = \Delta z_0 \tag{3.31}$$

$$-2\Delta\dot{x}_0 = \Delta\dot{z}_0 \tag{3.32}$$

, and similarly for GCO formation flying the constraints for initial state are given in 3.33-3.34:

$$-\sqrt{3}\Delta x_0 = \Delta z_0 \tag{3.33}$$

$$-\sqrt{3}\Delta\dot{x}_0 = \Delta\dot{z}_0 \tag{3.34}$$

Then according to these constraints regarding to initialization, we choose an initial state in LVLH frame of deputy satellite as $\mathbf{x}_0 = [A_x \quad 0 \quad -2A_x \quad 0 \quad -2nA_x \quad 0]^T$ and $\mathbf{x}_0 = [A_x \quad 0 \quad -\sqrt{3}A_x \quad 0 \quad -2nA_x \quad 0]^T$ for PCO and GCO respectively.

The PCO and GCO formations indicate that deputy satellite will always move in a circle or elliptical trajectory with respect to chief satellite without perturbation and therefore it keep a minimum distance to chief satellite and achieve a bounded relative motion which would not drift away over time. Then, it guarantees a much safe space mission scenario of multiple satellites system. The motion of deputy and chief satellite in ECI frame and LVLH frame for PCO and GCO formation flying are plotted in Fig 3.6 and fig 3.7.

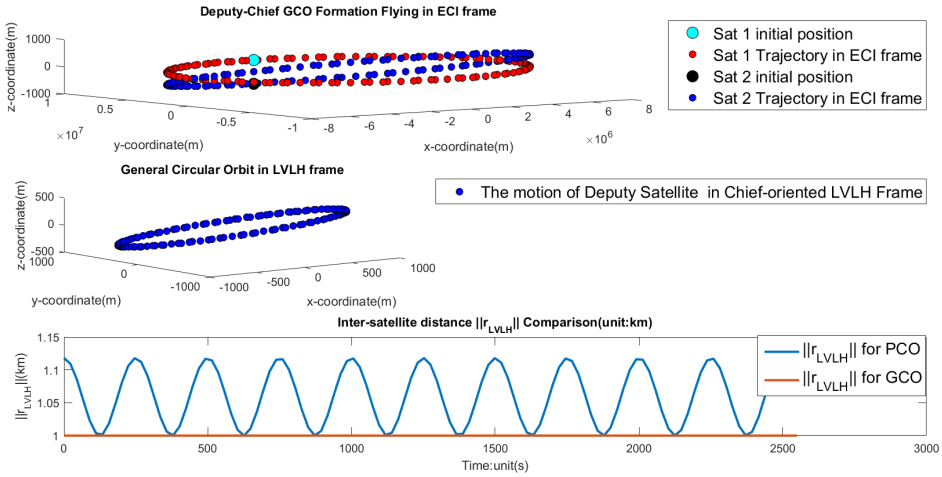

Figure 3.6: General Circular Orbit in ECI and LVLH frame

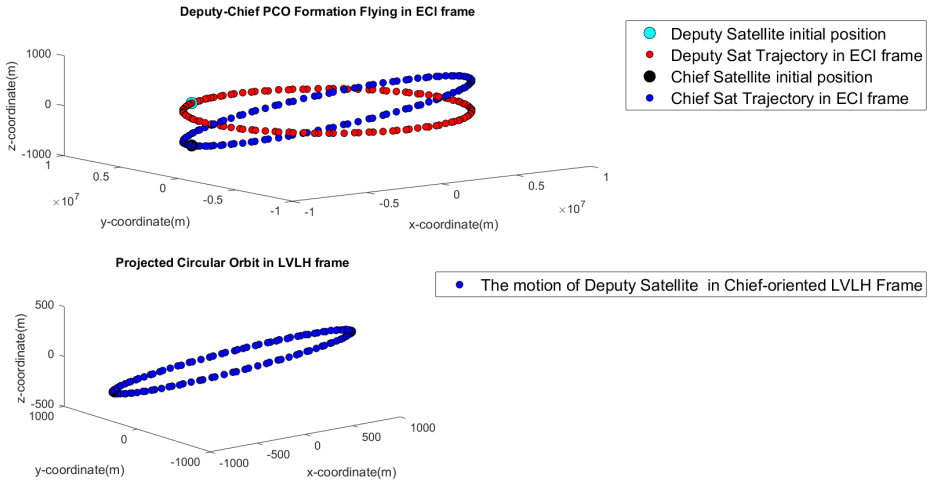

Figure 3.7: Projected Circular Orbit in ECI and LVLH frame

3.3 Triangular Satellite Formation

To extend the scenario of projected circular orbit for satellite formation with micro-satellite systems with more satellites, the triangular satellite formation strategy is applied. This scenario is quiet advantageously be applied in satellite-based laser interferometry that measure inter-satellite distance variation caused by gravitational waves [10] and Synthetic-Aperture-Radar (SAR) interferometry [5] to acquire remote sensing imaging that require larger image scale and also combine neighbouring images from different satellite cameras to analysis and construct ambient environment image data. Therefore, a question arises that how could we choose appropriate initialization of satellites position and velocity vectors in LVLH frame to generate orbits with same relative trajectory shape but different initial positions. Thereby, we consider three satellites could form a triangular satellite network that all move in a PCO trajectory in an virtual-reference-oriented LVLH frame. This virtual reference point is located in the center of PCO trajectory in Fig 3.8 and is same for all three satellites.

Thus for each individual satellite, recall (3.21) its relative motion in an virtual-reference-oriented LVLH frame can be described as below:

$$\Delta x(t) = A_x \cos(nt + \beta_x) \tag{3.35}$$

$$\Delta y(t) = -2A_x \sin(nt + \beta_x) + 2A_x \sin(\beta_x) + \Delta y_0 \tag{3.36}$$

$$\Delta z(t) = -2A_x \cos(nt + \beta_x) \tag{3.37}$$

3.3.1 In-plane Triangular Formation

From observation of (3.35)-(3.37), A_x should be same and constant for all three satellite to obtain same orbital shape:

$$A_x = \frac{-\Delta x_0}{\cos(\beta_x)} = const \tag{3.38}$$

Then, from analysis of solution corresponds to projected circular orbit in (3.35)-(3.37), the phase angle β_x or initial displacement in x-direction should be varied to let different satellites start moving at different positions, however, variation in phase angle will result in different shift of $2A_x sin(\beta_x) + \Delta y_0$ in along-track direction , if all satellites move in same PCO which means same A_x. Recall (3.31), (3.32) and (3.21) the initial state to generate PCO could be written as:

$$\mathbf{x}_0 = [\Delta x_0 \quad \Delta y_0 \quad -2\Delta x_0 \quad \Delta \dot{x_0} \quad -2n\Delta x_0 \quad -2\Delta \dot{x_0}]^T \tag{3.39}$$

β_x should be same to avoid different shifts in along-track direction, recall (3.22) and(3.24), it simply means Δx_0 and $\Delta \dot{x_0}$ should be same under same angular velocity n. In convenience, we set Δy_0 to 0 and thus the in-plane motion for three satellites can be formed that we vary mean anomaly under same initialization of deputy satellite state vector in chief-oriented LVLH frame, which means to generate one projected circular orbit with same initial position and velocity vectors for all three satellites but varying the launching time. This scenario is shown in Fig 3.8.

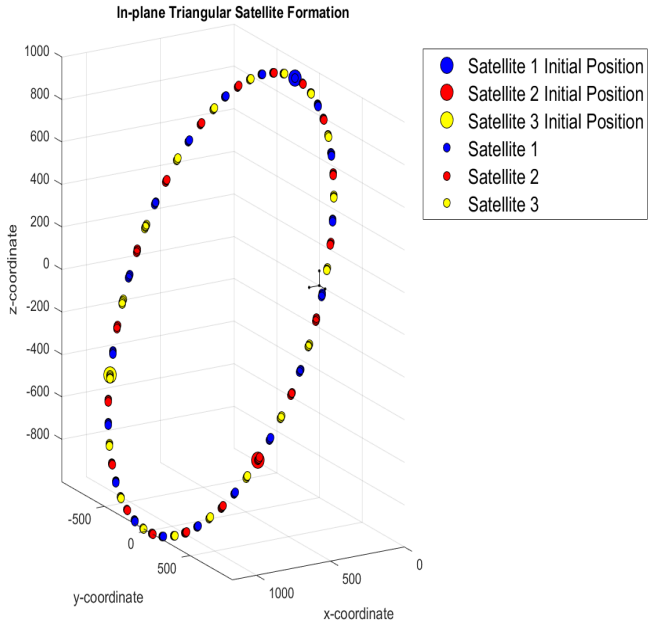

Figure 3.8: In-plane Triangular Satellite Formation

From above analysis, satellite network with more satellites can also form same relative orbital shape in same plane but shifted displacement in y-direction in LVLH frame shown in in fig 3.9, if they have different initial state in LVLH frame and thus cause different distance shifts in along-track direction.

This could be used in space rendzevous. As satellites move in parallel orbits and therefore we could connect different spacecrafts if they are separated sufficiently close with each other like Sat 2,3 in fig 3.9, where their initial positions are overlapped in y and z direction in LVLH frame. Also, as their orbits in LVLH frame are shifted by $2A_x sin(\beta_x) + \Delta y_0$ in y direction. Thus, a large Δy_0 will provide the advantage of collision avoidance and therefore we could shift their trajectory in LVLH frame arbitrarily to achieve different space mission requirements.

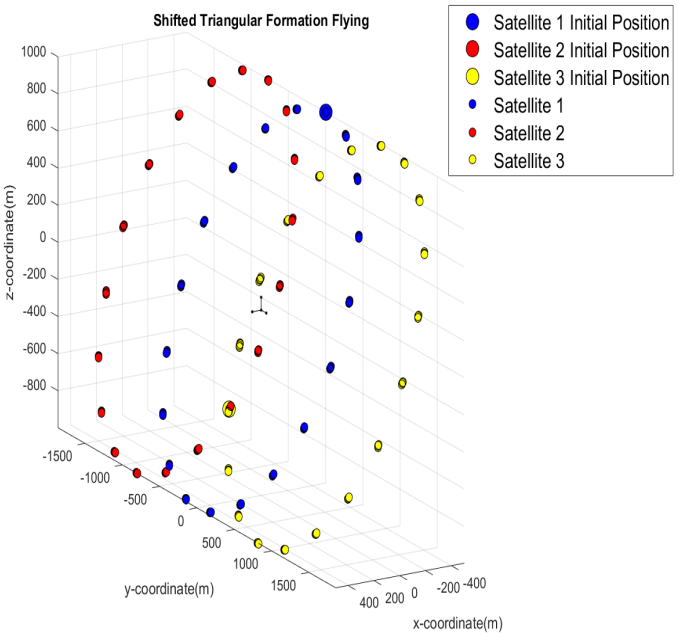

Figure 3.9: Shifted Triangular Satellite Formation

Chapter 4

Kalman Filter for Satellite Tracking

In this chapter, the Kalman Filter is introduced to deal with satellite tracking problem in LEO with presence of classic HCW dynamic model originated from HCW equations for a deputy-chief satellite network. Additionally, satellite tracking under atmospheric drag force and J2 perturbation are also discussed, which can be achieved with a Drag-modified linear dynamic model and apply Extended Kalman Filter to state estimation in a nonlinear J2 dynamics via a linearization of nonlinear system dynamic model.

4.1 The Introduction of Discrete-time Kalman Filter and its Principle

The Kalman Filter is a recursive estimator which is quite frequently used in the state estimation tasks with incorporation of noisy measurements for linear system [9]. This estimator is generally used in discrete form, since measurement from sensory components are always taking measurements discretely. The overall Kalman Filter model can be spilt into two parts: process model and measurement model. Firstly, we assume there is a linear time-invariant state transition model $\mathbf{F}_k$ and control input $\mathbf{u}_k$ with gain $\mathbf{G}_k$ that maps state of a dynamic system at given time step $k-1$ $\mathbf{C}_{k-1}$ to next step step $\mathbf{C}_k$. The various noise sources as well as model inaccuracies are modeled by the process noise w_k. Thus, the state at time instance k is given by the combination of mapping with linear state transition model and process noises $\mathbf{w}_k$ [9]:

$$\mathbf{C}_k = \mathbf{F}_k\mathbf{C}_{k-1} + \mathbf{G}_k\mathbf{u}_k + \mathbf{w}_k \tag{4.1}$$

Certainly, a series of measurement data are required for estimation. Similarly, an observation matrix $\mathbf{H}_k$ is used to map true state space into observation space. Thus, the measurement model is used to obtain our state measurement based on this mapping from some measurement acquisition tools like sensors and observation noises $\mathbf{m}_k$ (from ambient environment and sensors), when measurement are taken at a given time step. This is described as (4.2):

$$\mathbf{L}_k = \mathbf{H}_k\mathbf{x}_k + \mathbf{m}_k \tag{4.2}$$

The process noise and observation noise are assumed to be uncorrelated zero-mean Gaussian distributed with given noise variance: the elements $m_{i,k}$ and $w_{i,k}$ in $\mathbf{m}_k$ and vector $\mathbf{w}_k$ have variance σ_v^2 and σ_w^2 respectively. Meanwhile, $\mathbf{m}_k$ and $\mathbf{w}_k$ have a covariance matrix given by $\mathbf{R}_k = \sigma_v^2 \cdot \mathbf{I}$ and $\mathbf{Q}_k = \sigma_w^2 \cdot \mathbf{I}$, where $\mathbf{I}$ is the identity matrix of same dimension as the length of the

vector $\mathbf{w}_k$. The $\mathbf{Q}_k$ and $\mathbf{R}_k$ are process noise covariance matrix and observation noise covariance matrix at step k respectively. However, this is not case in real scenario, where process noise and observation noise variance may vary. But in this thesis, we don't consider this for simplification. The Kalman Filter can be explained as a set of mathematical equations. The diagram in Fig 4.1 shows its principle. Firstly we calculate a prior state estimate at time step k $\mathbf{C}_{k|k-1}$ and predict error covariance estimate $\mathbf{P}_{k|k-1}$ based on our system model $\mathbf{F}_k$ and process noise covariance. The predict error covariance matrix contains covariance of a posterior estimation error and describes how close the a posterior estimated state to the true state, which could reflect estimation accuracy. This phase we call prediction. Then we proceed to the calculation of residual $\mathbf{d}_k$, which is difference between actual noisy observation $\mathbf{L}_k$ from linear observation model and the estimated observation based on a prior state estimate $\mathbf{C}_{k|k-1}$. Afterwards, the Kalman gain $\mathbf{K}_k$ is calculated as a manner to adaptively minimize the trace of a posterior predict error covariance matrix $trace(\mathbf{P}_{k|k})$. This is also equivalent as minimize expectation as $\text{argmin}(\mathcal{E}(\mathbf{e}_k\mathbf{e}_k^T))$, where $\mathbf{e}_k$ is a posterior estimation error and calculated as difference between true state $\mathbf{C}_k$ and a posterior state estimate $\mathbf{C}_{k|k}$ at time step k:

$$\mathbf{e}_k = \mathbf{C}_k - \mathbf{C}_{k|k} \tag{4.3}$$

The overall estimation process is given as [9]:

$$\mathbf{C}_{k|k-1} = \mathbf{F}_k\mathbf{C}_{k-1|k-1} + \mathbf{G}_k\mathbf{u}_k \tag{4.4}$$

$$\mathbf{P}_{k|k-1} = \mathbf{F}_k\mathbf{P}_{k-1|k-1}\mathbf{F}_k^T + \mathbf{Q}_k \tag{4.5}$$

$$\mathbf{d}_k = \mathbf{L}_k - \mathbf{H}_k\mathbf{C}_{k|k-1} \tag{4.6}$$

$$\mathbf{K}_k = \mathbf{P}_{k|k-1}\mathbf{H}_k^T(\mathbf{H}_k\mathbf{P}_{k|k-1}\mathbf{H}_k^T + \mathbf{R}_k)^{-1} \tag{4.7}$$

$$\mathbf{C}_{k|k} = \mathbf{C}_{k|k-1} + \mathbf{K}_k\mathbf{d}_k \tag{4.8}$$

$$\mathbf{P}_{k|k} = (\mathbf{I} - \mathbf{K}_k\mathbf{H}_k)\mathbf{P}_{k|k-1} \tag{4.9}$$

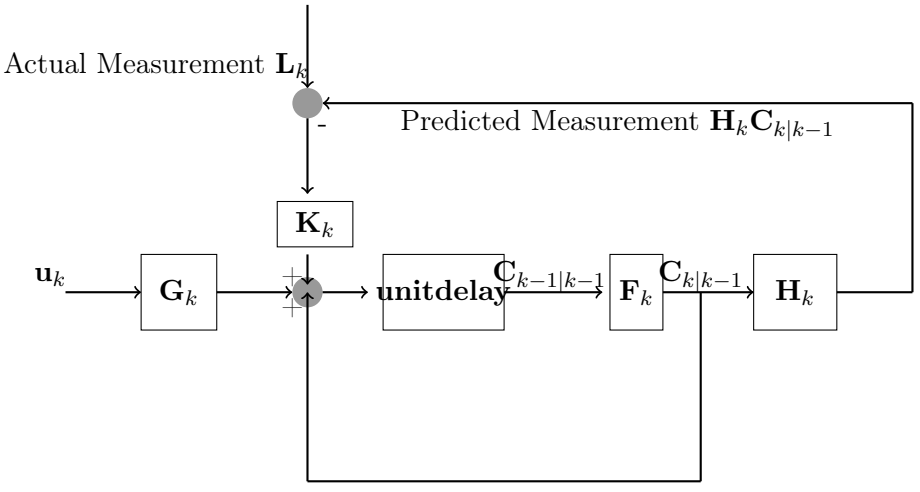

Figure 4.1: Kalman Filter Algorithm Illustration

Then we proceed to update the state and predict error co-variance matrix at time-step k as $\mathbf{C}_{k|k}$ and $\mathbf{P}_{k|k}$ with calculated Kalman gain $\mathbf{K}_k$ and residual $\mathbf{d}_k$. Finally, Kalman gain and predict error covariance matrix will stabilize and this means Kalman Filter is converged and then the mean square error $||\mathbf{e}_k||$ will be minimized and converged with increasing time instance k.

4.2 Kalman Filter State Estimation for Unperturbed Satellite Motion

4.2.1 Position and Velocity Estimation with HCW Model

In this part we use Kalman Filter to track deputy satellite's position and velocity, which is orbiting in a projected circular orbit in the chief-oriented LVLH frame. Then we could navigate satellite and also optimize its trajectory based on our estimation. In order to implement it, the dynamic system model and the observation model should be firstly considered, thus from the previous HCW equations we are able to construct a linear dynamic system model with state vector of deputy satellite $\mathbf{x}(t)$ in chief-oriented LVLH frame that describes relative motion of deputy-chief satellite system as below:

$$\underbrace{\begin{pmatrix} \Delta\dot{x}(t) \\ \Delta\dot{y}(t) \\ \Delta\dot{z}(t) \\ \Delta\ddot{x}(t) \\ \Delta\ddot{y}(t) \\ \Delta\ddot{z}(t) \end{pmatrix}}_{\dot{\mathbf{x}}(t)} = \underbrace{\begin{pmatrix} 0 & 0 & 0 & 1 & 0 & 0 \\ 0 & 0 & 0 & 0 & 1 & 0 \\ 0 & 0 & 0 & 0 & 0 & 1 \\ 3n^2 & 0 & 0 & 0 & 2n & 0 \\ 0 & 0 & 0 & -2n & 0 & 0 \\ 0 & 0 & -n^2 & 0 & 0 & 0 \end{pmatrix}}_{\mathbf{F}_{HCW}} \cdot \underbrace{\begin{pmatrix} \Delta x(t) \\ \Delta y(t) \\ \Delta z(t) \\ \Delta\dot{x}(t) \\ \Delta\dot{y}(t) \\ \Delta\dot{z}(t) \end{pmatrix}}_{\mathbf{x}(t)} \tag{4.10}$$

This dynamic model can be represented as:

$$\dot{\mathbf{x}}(\mathbf{t}) = \mathbf{F}_{HCW} \cdot \mathbf{x}(\mathbf{t}) \tag{4.11}$$

To apply discrete-time Kalman Filter, a discretization of time-continuous HCW model in (4.11) must be done. Firstly, we consider two subsequent deputy satellite state vectors $\mathbf{x}_{k+1}$ and $\mathbf{x}_k$. The $\dot{\mathbf{x}}(t)$ could be written as:

$$\dot{\mathbf{x}}(t) = \frac{\mathbf{x}_{k+1} - \mathbf{x}_k}{\Delta t} \tag{4.12}$$

, $\dot{\mathbf{x}}(t)$ could be represented as left side of (4.13) from (4.11) , thus we get:

$$\frac{\mathbf{x}_{k+1} - \mathbf{x}_k}{\Delta t} = \mathbf{F}_{HCW} \cdot \mathbf{x}_k \tag{4.13}$$

, as we should plus process noise $\mathbf{w}_k$ to account for noises from ambient environment and sensor etc, after rearrangement we get:

$$\mathbf{x}_{k+1} = \underbrace{(\Delta t \mathbf{F}_{HCW} + \mathbf{I}_{\mathbf{6}\times\mathbf{6}})}_{\mathbf{F}} \cdot \mathbf{x}_k + \mathbf{w}_k \tag{4.14}$$

, where Δt is time interval between step k and step $k+1$. Also, a linear observation model is constructed as below:

$$\mathbf{L}_k = \mathbf{I}_{6\times 6} \cdot \mathbf{x}_k + \mathbf{m}_k \tag{4.15}$$

where $\mathbf{I}_{6\times 6}$ is 6×6 identity matrix.

4.3 Kalman Filter with Perturbation

4.3.1 Drag-modified HCW Model

In the deputy-chief satellite scenario, the motion equation include drag force for chief satellite can be represented as [6]:

$$\ddot{\boldsymbol{r}}_d = -f(||\boldsymbol{r}_d||)\boldsymbol{r}_d - \alpha g(||\boldsymbol{r}_d||)||\boldsymbol{r}_d||\boldsymbol{r}_d \tag{4.16}$$

Also for deputy satellite:

$$\ddot{\boldsymbol{r}}_f = -f(||\boldsymbol{r}_f||)\boldsymbol{r}_f - \psi g(||\boldsymbol{r}_f||)||\boldsymbol{r}_f||\boldsymbol{r}_f \tag{4.17}$$

where $\boldsymbol{r}_d$ and $\boldsymbol{r}_f$ are position vectors of both satellites in ECI frame. (4.16) can be interpreted as acceleration of deputy satellite is the combination of gravitational acceleration $(-f(||\boldsymbol{r}_d||)\boldsymbol{r}_d)$ and acceleration from atmospheric drag force $(-\alpha g(\boldsymbol{r}_d)||\boldsymbol{r}_d||\boldsymbol{r}_d)$. This is similar for (4.17). ψ and α are drag constants for deputy and chief satellite respectively. $g(||\boldsymbol{r}_d||)$ and $g(||\boldsymbol{r}_f||)$ is atmospheric density function for chief and deputy satellites which is inversely proportional to $||\boldsymbol{r}_d||$ and $||\boldsymbol{r}_f||$ as:

$$g(||\boldsymbol{r_d}||) = \frac{1}{||\boldsymbol{r_d}||} \tag{4.18}$$

$$g(||\boldsymbol{r_f}||) = \frac{1}{||\boldsymbol{r_f}||} \tag{4.19}$$

and $f(||\boldsymbol{r_d}||)$ and $f(||\boldsymbol{r_d}||)$ is gravitational force:

$$f(||\boldsymbol{r}_d|| = \frac{GM}{||\boldsymbol{r}_d||^3}) \tag{4.20}$$

$$f(||\boldsymbol{r}_f|| = \frac{GM}{||\boldsymbol{r}_f||^3}) \tag{4.21}$$

Consider two satellites have a small relative distance and then we have $\boldsymbol{r}_f$=$\boldsymbol{r}_d$+$\boldsymbol{r}_{ECI}$ under condition of $||\boldsymbol{r}_{ECI}||\ll||\boldsymbol{r}_d||$. The relative acceleration vector $\ddot{\boldsymbol{r}}_{ECI}$ in ECI frame can be calculated as:

$$\ddot{\boldsymbol{r}}_{ECI} = \ddot{\boldsymbol{r}}_f - \ddot{\boldsymbol{r}}_d \tag{4.22}$$

Then, transforming $\ddot{\boldsymbol{r}}_{ECI} = [\ddot{x} \quad \ddot{y} \quad \ddot{z}]^T$ into the rotating LVLH frame, its solution could be represented as below, detailed derivation can be seen in reference [6]:

$$\ddot{x} = 2\dot{y} + ||\boldsymbol{r}_d||(\alpha g(||\boldsymbol{r}_d||) + \psi\dot{g}(||\boldsymbol{r}_d||)||\boldsymbol{r}_d||)y + (\psi - \alpha)g(||\boldsymbol{r}_d||)(2||\boldsymbol{r}_d||y - ||\dot{\boldsymbol{r}_d}||x + \frac{||\boldsymbol{r}_d||^2}{E(\theta)}) \tag{4.23a}$$

$$\ddot{y} = -2\dot{x} - (\frac{f(||\dot{\boldsymbol{r}_d}||)||\boldsymbol{r}_d||}{n^2} + \alpha g(||\boldsymbol{r}_d||)||\dot{\boldsymbol{r}_d}|| + \psi\dot{g}(||\boldsymbol{r}_d||)||\boldsymbol{r}_d||||\dot{\boldsymbol{r}_d}||)y - (\psi - \alpha)g(||\boldsymbol{r}_d||)((||\boldsymbol{r}_d||y)' - ||\dot{\boldsymbol{r}_d}||x + \tag{4.23b}$$

$$\frac{||\boldsymbol{r}_d||^2}{E(\theta)}) \tag{4.23c}$$

$$\ddot{z} = -z - (||\dot{\boldsymbol{r}_d}||z)(\psi - \alpha)g(||\boldsymbol{r}_d||) \tag{4.23d}$$

Assume identical drag constants ψ and α for two satellites. θ is polar angle. n is angular velocity of chief satellite. $E(\theta)$ is a transformation function for simplification and given as [6]:

$$E(\theta) = ||\boldsymbol{r}_d||^{-1}h^{0.5}e^{-\alpha\theta} \tag{4.24}$$

, where h is an integral constant, substitute (4.18), (4.24) and (4.20) into (4.23), then (4.23) can be reduced as:

$$\ddot{x} = 2\dot{y} \tag{4.25a}$$

$$\ddot{y} = 2\dot{x} + 3GMh^{-2}||\boldsymbol{r}_d||e^{2\alpha\theta}y \tag{4.25b}$$

$$\ddot{z} = -z \tag{4.25c}$$

for the initial circular orbit,

$$||\boldsymbol{r}_d|| = l_0e^{-2\alpha\theta} \tag{4.26}$$

where $l_0 = \frac{h^2(1+4\alpha^2)}{GM}$, therefore substitute this expression in (4.25), a modified linear dynamic model includes drag force is established as:

$$\underbrace{\begin{pmatrix}\Delta\dot{x}(t)\\ \Delta\dot{y}(t)\\ \Delta\dot{z}(t)\\ \Delta\ddot{x}(t)\\ \Delta\ddot{y}(t)\\ \Delta\ddot{z}(t)\end{pmatrix}}_{\dot{\mathbf{x}}(t)} = \underbrace{\begin{pmatrix}0 & 0 & 0 & 1 & 0 & 0\\ 0 & 0 & 0 & 0 & 1 & 0\\ 0 & 0 & 0 & 0 & 0 & 1\\ 0 & 0 & 0 & 0 & 2 & 0\\ 0 & 3(1+4\alpha^2) & 0 & -2 & 0 & 0\\ 0 & 0 & -1 & 0 & 0 & 0\end{pmatrix}}_{\mathbf{F}_{drag}} \cdot \underbrace{\begin{pmatrix}\Delta x(t)\\ \Delta y(t)\\ \Delta z(t)\\ \Delta\dot{x}(t)\\ \Delta\dot{y}(t)\\ \Delta\dot{z}(t)\end{pmatrix}}_{\mathbf{x}(t)} \tag{4.27}$$

, also the discrete form can be given follow same method used in the previous classic HCW model case:

$$\mathbf{x}_{k+1} = \underbrace{(\Delta t\mathbf{F}_{drag} + \mathbf{I}_{\mathbf{6}\times\mathbf{6}})}_{\mathbf{F_d}} \cdot \mathbf{x}_k + \mathbf{w}_k \tag{4.28}$$

This model is very accurate for satellite with very small drag constants, since in this simplied drag HCW model, atmospheric density depends on altitude for both satellites is modelled as inverse law in (4.18) and (4.19). However, in reality it decreases exponentially which follows

barometric formula given by (2.24). Therefore, for very small drag constants, we can ignore error of modelling atmospheric density variation between two satellites with inverse law, where it has non-negligible error produced for large drag constants. Therefore, we set $\alpha = 2.2e-3$ for simulation.

4.3.2 The Extended Kalman Filter (EKF) Introduction

The classic Kalman Filter is applied for state estimation due to the fact of that the target system is linear time-invariant under unperturbed scenarios. But when some perturbations is included in the model itself, state transition model $\mathbf{F}_k$ will follow nonlinear variations and is described by nonlinear differentiable function $f_k(\mathbf{x}_k)$ and this is most cases in reality. Also, in some cases observation model at step $k+1$ $\mathbf{H}_{k+1}$ cannot be linear and could be written as differentiable function $h_{k+1}(\mathbf{x}_{k+1})$. Therefore,the Extended Kalman Filter (EKF) is came up with to tackle nonlinearities in the model, it is done by linearizing state transition function $f_k(\mathbf{x}_k)$ and observation model $h_{k+1}(\mathbf{x}_{k+1})$ to get Jacobian matrices at two working points, one at a-posterior estimate $\mathbf{x}_{k|k}$ the other one at a-prior estimate $\mathbf{x}_{k+1|k}$ by expanding the Taylor series of $f_k(\mathbf{x}_{k|k})$ and $h_{k+1}(\mathbf{x}_{k+1|k})$ and take the first two terms and neglect higher order terms $\mathbf{o}(n)$ as [9]:

$$f_k(\mathbf{x}_k) = f_k(\mathbf{x}_{k|k}) + \frac{\partial f_k(\mathbf{x}_{k|k})}{\partial \mathbf{x}_{k|k}}(\mathbf{x}_k - \mathbf{x}_{k|k}) + \mathbf{o}(n) \tag{4.29}$$

$$h_{k+1}(\mathbf{x}_{k+1}) = h_{k+1}(\mathbf{x}_{k+1|k}) + \frac{\partial h_{k+1}(\mathbf{x}_{k+1|k})}{\partial \mathbf{x}_{k+1|k}}(\mathbf{x}_{k+1} - \mathbf{x}_{k+1|k}) + \mathbf{o}(n) \tag{4.30}$$

Then, under nonlinear effects the true state and system observation at time step $k+1$ $\mathbf{x}_k$ and $\mathbf{y}_{k+1}$ can be written as:

$$\mathbf{x}_{k+1} = f_k(\mathbf{x}_k) + \mathbf{w}_k \tag{4.31}$$

$$\mathbf{y}_{k+1} = h_{k+1}(\mathbf{x}_{k+1}) + \mathbf{m}_{k+1} \tag{4.32}$$

Subsequently, above two equations could be rewritten after substitutions of (4.29) and (4.30) into (4.31)-(4.32).

$$\mathbf{x}_{k+1} = \frac{\partial f_k(x_{k|k})}{\partial \mathbf{x}_{k|k}}\mathbf{x}_k + \mathbf{w}_k + \mathbf{s}_k \tag{4.33}$$

$$\mathbf{y}_{k+1} = \frac{\partial \mathbf{h}_{k+1}(\mathbf{x}_{k+1|k})}{\partial \mathbf{x}_{k+1|k}}\mathbf{x}_{k+1} + \mathbf{m}_{k+1} + \mathbf{t}_{k+1} \tag{4.34}$$

where $\mathbf{s}_k = f_k(\mathbf{x}_{k|k}) - \frac{\partial f_k(\mathbf{x}_{k|k})}{\partial \mathbf{x}_{k|k}}\mathbf{x}_{k|k}$ and $\mathbf{t}_{k+1} = h_{k+1}(\mathbf{x}_{k+1|k}) - \frac{\partial h_k(\mathbf{x}_{k+1|k})}{\partial \mathbf{x}_{k+1|k}}\mathbf{x}_{k+1|k}$ and they depend on previous a posterior state estimate $\mathbf{x}_{k|k}$ and current a prior state estimate $\mathbf{x}_{k+1|k}$. Then a nonlinear system and observation are approximated to be linear given by (4.33)-(4.34) and offers us a way to deal with state estimation problems with conventional Kalman Filter.

4.3.3 J2-modified HCW Equations and the Solutions

In spite of drag force, it is also important to investigate how Earth in-homogeneous gravitational field majorly J2 term will affect KF performance and therefore the navigation accuracy of satellite

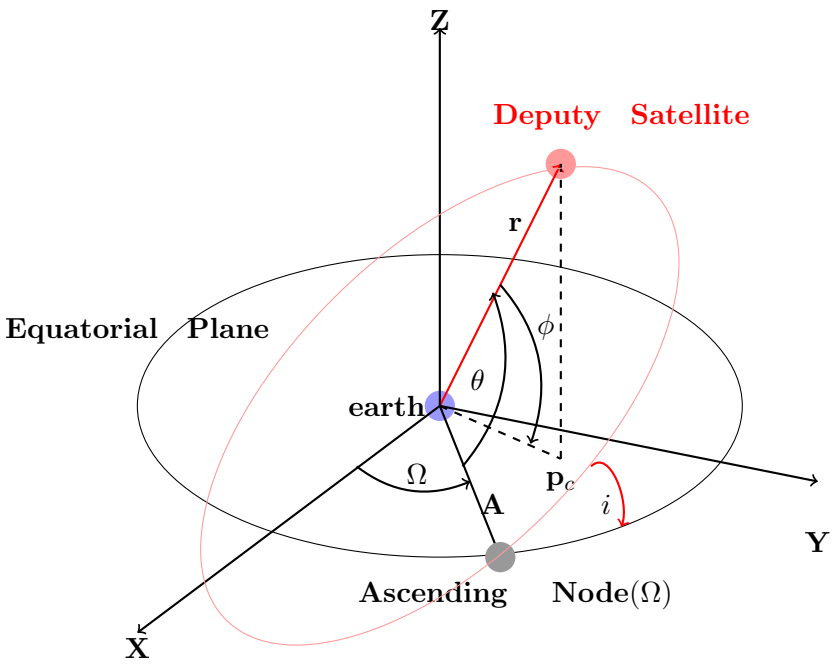

Figure 4.2: Chief Orbital Elements

in LEO. Therefore, establishing a J2-modified nonlinear HCW equation should be considered as priority. Recall gravitational potential representation in (2.20)-(2.21). The disturbing potential in relation to a given geocentric latitude ϕ from J2 term is given in spherical coordinates:

$$V_{J2} = \frac{GM}{||\mathbf{r}||^3} J_2 (\frac{a_e}{r})^2 P_2(\sin(\phi))) \tag{4.35}$$

, from Fig 4.2, the relation of inclination angle i, polar angle θ and ϕ is given as:

$$||\mathbf{r}|| \sin(\phi) = ||\mathbf{r}|| \sin(\theta) \sin(i) \tag{4.36}$$

, then the Legendre polynomial with second order $P_2(\sin(\phi))$ is given as [1]:

$$\begin{aligned} P_2(\sin(\phi)) =& \frac{1}{2}(1 - 3\sin(\phi)^2) \\ =& \frac{1}{2}(1 - 3\sin(i)^2 \sin(\theta)^2) \end{aligned} \tag{4.37}$$

, $\mathbf{p}_c$ is projection of deputy satellite in the equatorial plane shown in Fig 4.2. For circular orbit, θ can be approximated as $n \cdot t$. where n is angular velocity of deputy satellite. Then, it is reasonable to insert (4.37) into (4.35) and calculate partial derivative of potential V_{J2} and transform it into rotating LVLH frame to get additional acceleration components caused by J2 perturbation for HCW equations [0]:

$$\Delta\ddot{x} = 3n^2\Delta x + 2n\Delta\dot{x} - j(1 - 3\sin(i)^2\sin(\theta)^2) \tag{4.38a}$$
$$\Delta\ddot{y} = -2n\Delta\dot{y} - 2j\sin(\theta)\cos(\theta)) \tag{4.38b}$$
$$\Delta\ddot{z} = -n^2\Delta z - 2j(\sin(i)\cos(i)\sin(\theta)) \tag{4.38c}$$

where $j = \frac{3GMa_e^2J_2}{2||\mathbf{r}||^4}$, then a J2-modified HCW model can be constructed as:

$$\underbrace{\begin{pmatrix}\Delta\dot{x}(t)\\ \Delta\dot{y}(t)\\ \Delta\dot{z}(t)\\ \Delta\ddot{x}(t)\\ \Delta\ddot{y}(t)\\ \Delta\ddot{z}(t)\end{pmatrix}}_{\dot{\mathbf{x}}(t)} = \underbrace{\begin{pmatrix}0 & 0 & 0 & 1 & 0 & 0\\ 0 & 0 & 0 & 0 & 1 & 0\\ 0 & 0 & 0 & 0 & 0 & 1\\ 3n^2 & 0 & 0 & 0 & 2n & 0\\ 0 & 0 & 0 & -2n & 0 & 0\\ 0 & 0 & -n^2 & 0 & 0 & 0\end{pmatrix}}_{\mathbf{F}_{HCW}} \cdot \underbrace{\begin{pmatrix}\Delta x(t)\\ \Delta y(t)\\ \Delta z(t)\\ \Delta\dot{x}(t)\\ \Delta\dot{y}(t)\\ \Delta\dot{z}(t)\end{pmatrix}}_{\mathbf{x}(t)} + \mathbf{u}_{J2} \tag{4.39}$$

where $\mathbf{u}_{J2} = \begin{bmatrix}0\\ 0\\ 0\\ -j(1-3\sin(i)^2\sin(\theta)^2)\\ -2j\sin(\theta)\cos(\theta))\\ -2j\sin(i)\cos(i)\cos(\theta))\end{bmatrix}$

Therefore, recall original discrete form of HCW model, a new HCW dynamic model in discrete form can be represented as:

$$\begin{aligned}\mathbf{x_{k+1}} &= \underbrace{(\Delta t\mathbf{F})_{\mathbf{HCW}} + I_{6\times6})\mathbf{x_k} + \Delta t\mathbf{u}_{J2}}_{f_{J2}(\mathbf{x}_k)} + \mathbf{w}_k \\ &= f_{J2}(\mathbf{x}_k) + \mathbf{w}_k\end{aligned} \tag{4.40}$$

With the existence of nonlinearities in process model (f_{j2}), an extended Kalman Filter is applied with assumption that the variation of nonlinear noise caused by J2 perturbation varies smoothly. The observation model remains the same as unperturbed case, to reduce nonlinearity in the system and make it less complicated to solve. The following evaluation process is considered with presence of linear observation model given as [9]:

$$\mathbf{x}_{k+1|k} = f_{J2}(\mathbf{x}_{k|k}) \tag{4.41a}$$
$$\mathbf{P}_{k+1|k} = \mathbf{F}_{J2-(k)}P_{k|k}\mathbf{F}_{J2-(k)}^T + \mathbf{Q}_k \tag{4.41b}$$
$$\mathbf{L}_{k+1} = \mathbf{I}_{6\times6}\cdot\mathbf{x}_{k+1} + \mathbf{m}_{k+1} \tag{4.41c}$$
$$\mathbf{d}_{k+1} = \mathbf{L}_{k+1} - \mathbf{I}_{6\times6}\mathbf{x}_{k+1|k} \tag{4.41d}$$
$$\mathbf{K}_{k+1} = \mathbf{P}_{k+1|k}\mathbf{I}_{6\times6}^T(\mathbf{I}_{6\times6}\mathbf{P}_{k+1|k}\mathbf{I}_{6\times6}^T + \mathbf{R}_{k+1})^{-1} \tag{4.41e}$$
$$\mathbf{x}_{k+1|k+1} = \mathbf{x}_{k+1|k} + \mathbf{K}_{k+1}\mathbf{d}_{k+1} \tag{4.41f}$$
$$\mathbf{P}_{k+1|k+1} = (\mathbf{I}_{6\times6} - \mathbf{K}_{k+1}\mathbf{I}_{6\times6})\mathbf{P}_{k+1|k} \tag{4.41g}$$

where: $\mathbf{F}_{J2-(k)} = \frac{\partial f_{J2}(\mathbf{x})}{\partial \mathbf{x}}\Big|_{\mathbf{x}=\mathbf{x}_{k|k}}$

Chapter 5

State Estimation Results Analysis

In this chapter, we analysis the state estimation performance for one deputy satellite moving in an approximated projected circular orbit for three different scenarios: deputy satellite moving in an approximated projected circular orbit without perturbation and with atmospheric drag force and J2 perturbation with given initial state vectors in chief-oriented LVLH frame in table 5.1. The initial ECI position and velocity coordinates of chief satellite is set as $\mathbf{x}_{ECI} = [6.4046e6m \quad 0m \quad 0m \quad 0m/s \quad 0m/s \quad 7.889e3m/s]^T$. This is specifically chosen to maintain a circular orbit that fulfill assumption of HCW equation and a much lower orbital height so that perturbation have significant influence on satellite motion.

	$\mathbf{r}$(m)	$\mathbf{v}$(m/s)
Deputy Satellite(LVLH)	$[166.7\ 0\ 1000]^T$	$[0\ -0.3788\ 0]^T$
Chief Satellite(LVLH)	$[0\ 0\ 0]^T$	$[0\ 0\ 0]^T$
Deputy Satellite(ECI)	$[6.4056e6\ 166.67\ 6.12e\text{-}14\ ]^T$	$[2.51e\text{-}17\ -1.54e\text{-}33\ 7888.59]^T$
Chief Satellite(ECI)	$[6.4046e6\ 0\ 0]^T$	$[0\ 0\ 7.889e3]^T$

Table 5.1: Initial State Parameters of deputy and chief satellites in LVLH and ECI frame

Initial Parameter Setting

Initially to observe KF convergence process and we don't have knowledge of satellite motion state and need to estimate it. Therefore our initial estimate $\mathbf{x}_0$ is very bad and chosen randomly $\mathbf{x}_0 = [x_1, x_2, \ldots, x_6]^T$, where each element is uniformly distributed as $x_i \sim \mathcal{U}(0, 1)$

Process and observation noises are introduced into Kalman Filter. To analysis the effect of measurement noise variance σ_v^2 to the whole performance of Kalman Filter and consider the case in reality, where sensors also ambient environment will introduce much more noise and also the magnitude of true state norm, the simulated observation noise variance is appropriately chosen as σ_v^2 ranges from $2.714e2$ to $2.714e4$. Also, the elements in initial process noise $\mathbf{w}_k$ has variance σ_w^2 of $2.714e2$. The initial predict error covariance matrix $\mathbf{P}_{0|0}$ is set as diagonal matrix with much small values as $\text{diag}(1.8e-1, 1.8e-1, 1.8e-1, 18e-6, 18e-6, 18e-6)$. This is done to to minimize its influence on Kalman Filter convergence for further analysis because both $\mathbf{P}_{0|0}$ and process noise will affect estimated predict error covariance matrix $\mathbf{P}_{k+1|k}$ and then affect Kalman gain. All above parameters are same except process and observation noise levels for discussion in this chapter.

The error should be spilt into two parts: position and velocity estimation error E_{r-k} and E_{v-k}. For both cases, we calculated the norm of estimated and true position and velocity vectors at time step k of ith simulation $||\mathbf{r}_{(k|k)-i}||$, $||\mathbf{r}_{k-i}||$, $||\mathbf{v}_{(k|k)-i}||$ and $||\mathbf{v}_{k-i}||$ and the estimation error is defined as:

$$\hat{E_{r-i-k}} = 10\log\left(\mathcal{E}\left(\frac{(||\mathbf{r}_{k-i} - \mathbf{r}_{(k|k)-i}||)^2}{||\mathbf{r}_{k-i}||^2}\right)\right) \tag{5.1}$$

$$\hat{E_{v-i-k}} = 10\log\left(\mathcal{E}\left(\frac{(||\mathbf{v}_{k-i} - \mathbf{v}_{(k|k)-i}||)^2}{||\mathbf{v}_{k-i}||^2}\right)\right) \tag{5.2}$$

where $\hat{E_{r-i-k}}$ and $\hat{E_{v-i-k}}$ are position and velocity estimation error for ith simulation at time instance k , and $\mathcal{E}$ represents expected value. Instead of generating true state from HCW equations solutions that corresponds to a projected circular orbit with specific position and velocity vector initialization in LVLH frame. We replace true state as summation of HCW model plus zero-mean random Gaussian distributed noises $\mathbf{w}_k \sim \mathcal{N}(0, \mathbf{Q}_k)$ which shown in (5.3). This is because there may be model mismatch occurs, if we use true state from discretization of HCW model in continuous form in (4.14), which would not corresponds to a standard projected circular orbit. Therefore, predict error covariance matrix $\mathbf{P}_{k|k}$ would not only contains expectation of mean squared estimation error vector $\mathcal{E}(\mathbf{e}_k\mathbf{e}_k)$, but may also contains the portion from model mismatch and hard to model. However, $\mathbf{P}_{k|k}$ will perfectly represent $\mathcal{E}(\mathbf{e}_k\mathbf{e}_k)$ and there is no model mismatch if we do following substitution and true state corresponds to an approximated projected circular orbit.

$$\mathbf{x}_k = \mathbf{F}\mathbf{x}_{k-1} + \mathbf{w}_k \tag{5.3}$$

where $\mathbf{x_{k-1}}$ and $\mathbf{x_k}$ are true state vector at time-step $k-1$ and k and $\mathbf{x}_k = [\mathbf{r}_k \quad \mathbf{v}_k]^T$.

5.1 State Estimation Analysis of Classic HCW Model

The estimation behaviour to track a satellite in an approximated projected circular orbit are plotted in Fig 5.1. One important point should be noted is we run $N = 300$ simulations and calculate the average estimation error of all those 300 simulations to average noise effects due to random process from $\mathbf{w}_k$.

$$E_{r-k} = \frac{\sum_{i=1}^{N} \hat{E_{r-i-k}}}{N} \tag{5.4}$$

$$E_{v-k} = \frac{\sum_{i=1}^{N} \hat{E_{v-i-k}}}{N} \tag{5.5}$$

, where E_{r-k} and E_{v-k} are estimation error at time instance k after averaging for total N realizations. Then we spilt Kalman gain, residual, observation noise, actual measurement and true state for ith simulation at time instance k into position and velocity portions for further analysis as:

$$\mathbf{d}_{k-i} = [\mathbf{d}_{r-k-i} \quad \mathbf{d}_{v-k-i}]^T \tag{5.6}$$

$$\mathbf{K}_{k-i} = [\mathbf{K}_{r-k-i} \quad \mathbf{K}_{v-k-i}]^T \tag{5.7}$$

$$\mathbf{m}_{k-i} = [\mathbf{m}_{r-k-i} \quad \mathbf{m}_{v-k-i}]^T \tag{5.8}$$

$$\mathbf{x}_{k-i} = [\mathbf{r}_{k-i} \quad \mathbf{v}_{k-i}]^T \tag{5.9}$$

$$\mathbf{L}_{k-i} = [\mathbf{L}_{r-k-i} \quad \mathbf{L}_{v-k-i}]^T \tag{5.10}$$

Recall (5.4), it is feasible to calculate averaged position estimation error as below:

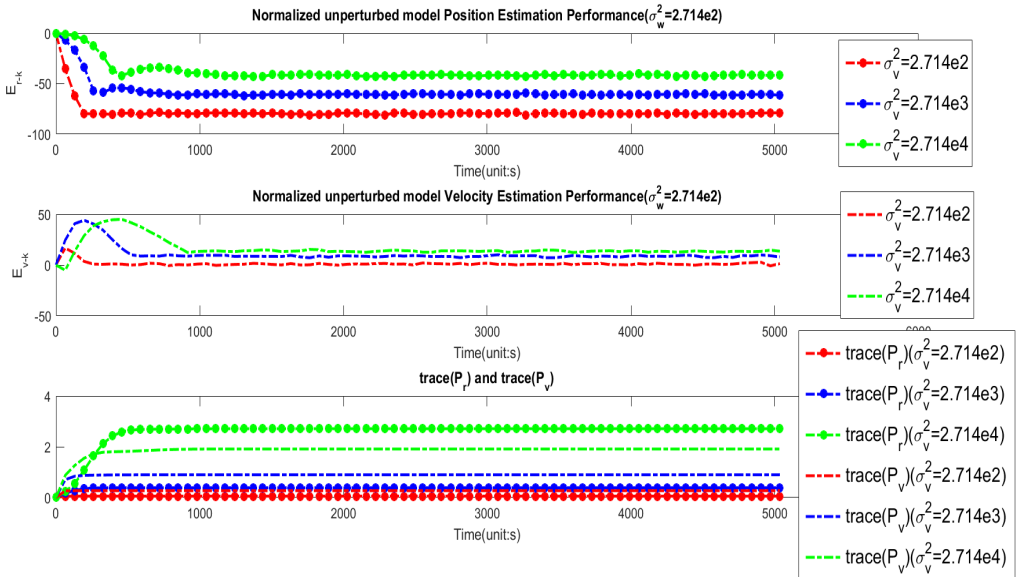

Figure 5.1: Kalman Filter Estimation Performance with Classic HCW Model

$$\begin{aligned} E_{r-k} &= \frac{1}{N}\sum_{i=1}^{N} 20\log\left(\mathcal{E}\left(\frac{||\mathbf{r}_{k-i} - \mathbf{r}_{(k|k)-i}||}{||\mathbf{r}_{k-i}||}\right)\right) \\ &= \frac{1}{N}\sum_{i=1}^{N} 20\log\left(\mathcal{E}\left(\frac{||\mathbf{r}_{k-i} - \mathbf{r}_{(k|k-1)-i} - \mathbf{K}_{r-k-i}\mathbf{d}_{k-i}||}{||\mathbf{r}_{k-i}||}\right)\right) \end{aligned} \tag{5.11}$$

, where $\mathbf{r}_{k-i}$, $\mathbf{r}_{(k|k)-i}$, $\mathbf{r}_{(k|k-1)-i}$ are true position vector, a posterior estimated position vector and a prior estimated position vector for ith simulation at time instance k respectively. Recall (4.15) and rearrange (4.6), write a prior position state estimate $\mathbf{r}_{(k|k-1)-i}$ as:

$$\begin{aligned} \mathbf{r}_{(k|k-1)-i} &= \mathbf{L}_{r-k-i} - \mathbf{d}_{r-k-i} \\ &= \mathbf{r}_{k-i} + \mathbf{m}_{r-k-i} - \mathbf{d}_{r-k-i} \end{aligned} \tag{5.12}$$

, take (5.12) into (5.11), we get:

$$E_{r-k} = \frac{1}{N}\sum_{i=1}^{N} 20\log\left(\mathcal{E}\left(\frac{||\mathbf{m}_{r-k-i} + \mathbf{K}_{r-k-i}\mathbf{d}_{k-i} - \mathbf{d}_{r-k-i}||}{||\mathbf{r}_{k-i}||}\right)\right) \tag{5.13}$$

, similarly for velocity estimation error E_{v-k}, we have:

$$E_{v-k} = \frac{1}{N}\sum_{i=1}^{N} 20\log\left(\mathcal{E}\left(\frac{||\mathbf{K}_{v-k-i}\mathbf{d}_{k-i} - \mathbf{d}_{v-k-i} + \mathbf{m}_{v-k-i}||}{||\mathbf{v}_{k-i}||}\right)\right) \tag{5.14}$$

while $\mathbf{v}_{k-i}$ is true velocity vector for ith simulation at time instance k.

Clearly, the increasing observation noise $\mathbf{m}_{r-k-i}$ and $\mathbf{m}_{v-k-i}$ causes worse KF position and velocity estimation performance, which can be seen from (5.12)-(5.14) that larger observation noise leads to larger estimation error E_{r-k} and E_{v-k} and make current actual measurement more noisy and less trusted. The trace of predict error covariance is important to quantify Kalman Filter quality. To analyze it, we spilt residual and trace of predict error covariance matrix into position and velocity parts:

$$trace(\mathbf{P}_{k|k}) = trace(\mathbf{P}_r) + trace(\mathbf{P}_v) \tag{5.15}$$

, where $trace(\mathbf{P}_r)$, $trace(\mathbf{P}_r)$ and $trace(\mathbf{P}_{k|k})$ are averaged traces for N realizations. One point to be noted is the trace for position and velocity shown in Fig 5.1 is divided by their means of final averaged results over time. The larger position and velocity estimation error reflects $trace(\mathbf{P}_r)$ and $trace(\mathbf{P}_v)$ increases and converges to a larger value shown in the lower subfigure of Fig 5.1. Also, it reflects the Kalman Filter convergence, as Kalman gain $\mathbf{K}_k$ and predict error covariance matrix $\mathbf{P}_{k|k}$ are stabilized after convergence. Therefore, if $trace(\mathbf{P}_r)$ and $trace(\mathbf{P}_v)$ both converges which means $trace(\mathbf{P}_{k|k})$ converges and also indicates convergence of Kalman Filter. The velocity estimation is much worse than position estimation, since the true velocity vector magnitude is too small compare with true position vector magnitude shown in Fig 5.3. Thus it is much larger when we normalize it. The residual $\mathbf{d}_k$ is an important metric to reflect KF performance, as it represents how well actual measurement fits to estimated measurement and further influence a posterior state estimate which is summation of $\mathbf{K}_k\mathbf{d}_k$ and a prior estimate $\mathbf{x}_{k|k-1}$. To more precisely investigate it, we take position and velocity curves shown in green in the top and middle sub-figure shown in Fig 5.1 as an example. The simulated process and observation noise $\mathbf{w}_k$ and $\mathbf{m}_k$ have variance of 2.714e2 and 2.714e4 for this example.

To investigate it, firstly we write its expression after averaging over N different realizations under the condition of identity matrix for observation matrix $\mathbf{H}_k$ as:

$$\begin{aligned}
\mathbf{d}_k = \begin{bmatrix}\mathbf{d}_{r-k}\\ \mathbf{d}_{v-k}\end{bmatrix} &= \frac{1}{N}\sum_{i=1}^{N}[\mathbf{L}_{k-i} - \mathbf{x}_{(k|k-1)-i}] \\
&= \frac{1}{N}\sum_{i=1}^{N}[\mathbf{x}_{k-i} + \mathbf{m}_{k-i} - \mathbf{x}_{(k|k-1)-i}] \\
&= \frac{1}{N}\sum_{i=1}^{N}[\mathbf{F}(\mathbf{x}_{(k-1)-i} - \mathbf{x}_{(k-1|k-1)-i}) + \mathbf{m}_{k-i} + \mathbf{w}_{k-i}]
\end{aligned} \tag{5.16}$$

(5.16) shows that increasing a posterior state estimation error $||\mathbf{e}_{k-1}||$ causes larger residual norm $||\mathbf{d}_k||$. Therefore, large residual means bad estimate and KF performance as well. This also implies for ith simulation a posterior estimation error at step $k-1$ $||\mathbf{e}_{(k-1)-i}|| = ||\mathbf{x}_{(k-1)-i} - \mathbf{x}_{(k-1|k-1)-i}||$ will directly influence residual at next time step, then this residual causes variation in a posterior state estimation error at next time step $||\mathbf{e}_k||$ and repeat this process until simulation terminates. As we normalize a posterior position and velocity estimation error by true position and velocity vector norm $||\mathbf{r}_k||$ and $||\mathbf{v}_k||$, increasing $||\mathbf{e}_{k-1}||$ doesn't necessary results increasing estimation error. Thus, it is more precise to conclude that interaction between residual at one time step and estimation error at one step before, true state norm at current time step and current observation noise $\mathbf{m}_{k-i}$ produce an overall position and velocity estimation error

pattern in Fig 5.1. Also, the variation trend in $||\mathbf{d}_r||$ and $||\mathbf{d}_v||$ will majorly reflect variation trend in normalized position and velocity estimation error, as $||\mathbf{v}_k||$ and $||\mathbf{r}_k||$ vary little in Fig 5.3. This can be seen in the comparison between lower subfigure of Fig 5.2 and position and velocity estimation error curve shown in green in Fig 5.1. Also KF converges which also means $||\mathbf{d}_{r-k}||$ and $||\mathbf{d}_{v-k}||$ converges shown in Fig 5.2. To observe observation noise effect to residual $\mathbf{d}_k$, we simply remove observation noise $\mathbf{m}_k$ and define two metrics:

$$\begin{bmatrix}\mathbf{d}_{r-metric}\\ \mathbf{d}_{v-metric}\end{bmatrix} = \frac{1}{N}\sum_{i=1}^{N}[\mathbf{F}\underbrace{(\mathbf{x}_{(k-1)-i} - \mathbf{x}_{(k-1|k-1)-i})}_{e_{(k-1)-i}} + \mathbf{w}_{k-i}] \tag{5.17}$$

The variation of $||\mathbf{d}_{r-metric}||$ and $||\mathbf{d}_{v-metric}||$ is plotted in the top subfigure of Fig 5.2. From

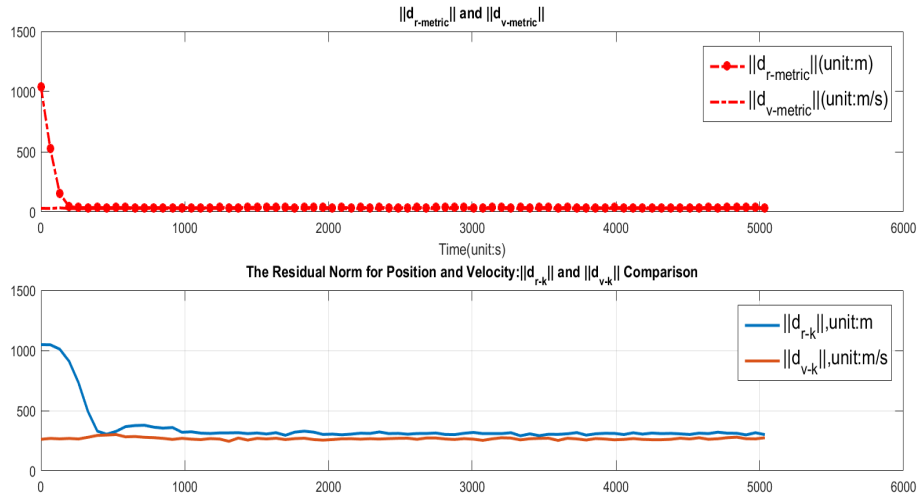

Figure 5.2: Residual Analysis Illustration

(5.16)-(5.17) and comparison between upper and lower subfigure of Fig 5.2, we discover that the presence of $\mathbf{m}_k$ results overall increase for $||\mathbf{d}_{r-k}||$ and for $||\mathbf{d}_{v-k}||$ in both convergent state and steady state, as $\mathbf{m}_k$ has a much larger variance (2.714e4) than $\mathbf{w}_k$ (2.714e2). This also corresponds to variation of position estimation and velocity estimation. The dramatic decrease of position estimation error and $||\mathbf{d}_{r-k}||$ at first stage is because Kalman gain is operated to minimize a posterior error covariance matrix, which is expectation of a posterior estimation error $\mathcal{E}(\mathbf{e}_k\mathbf{e}_k^T)$. Then KF converges and observation noise effect is minimized and residual converges which means actual measurement fit to estimated measurement to the largest extent and thus state estimation reaches best accuracy level.
The steady-state estimation error profile shows a very steady pattern, as we have averaged for random process from 300 different realizations of zero-mean random noise $\mathbf{w}_k$.

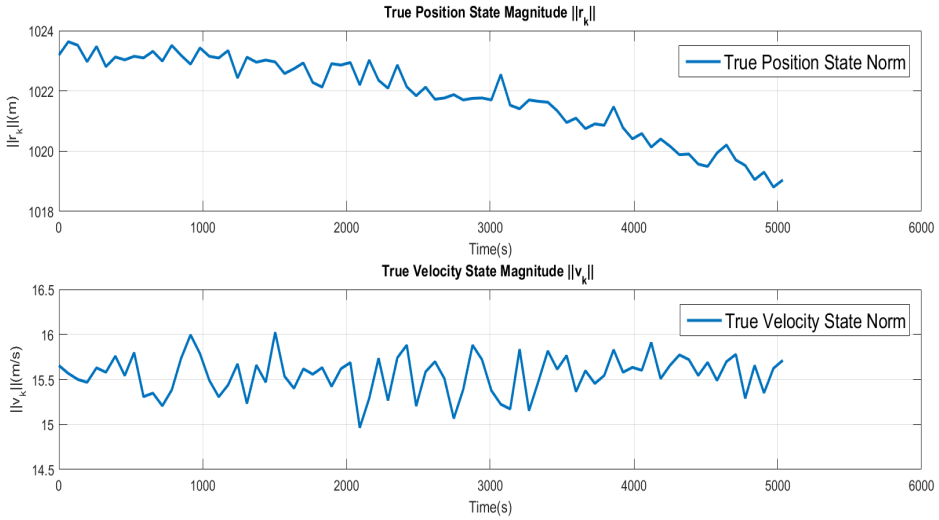

Figure 5.3: Averaged True Position and Velocity Magnitude of Deputy Satellite

5.2 KF Convergence Analysis

To analysis how process noise and observation noise influence KF convergence, different combinations of process noise and observation noise can be used to investigate their effects. Firstly, Kalman gain is closely related to KF convergence and in this case we simplify it with identity matrix as observation model:

$$\mathbf{K}_k = \mathbf{P}_{k|k-1}(\mathbf{P}_{k|k-1} + \mathbf{R}_k)^{-1} \tag{5.18}$$

Firstly, observation noise effect to convergence is discussed as below.
case 1: process noise variance σ_w^2 is larger than at least 10 times than observation noise variance σ_v^2: KF converges immediately shown in Fig 5.4, since recall (4.5) estimated predict error covariance $\mathbf{P}_{k|k-1}$ will depend on the level of process noise covariance $\mathbf{Q}_k$ with a very small initial value $\mathbf{P}_{0|0}$, thus Kalman gain $\mathbf{K}_k$ will be very close to identity matrix when $\mathbf{Q}_k$ is much larger than $\mathbf{R}_k$, predict error covariance matrix $\mathbf{P}_{k_k}$ will be very small. Thus Kalman Filter converges very fast.

case 2: process noise variance σ_w^2 is smaller at least 10 times than observation noise variance σ_v^2 shown as the scenario for three position and velocity estimation curves in Fig 5.5: KF converges slower with increasing σ_v^2 as shown in Fig 5.5, since observation noise covariance $\mathbf{R}_k$ dominates the level of Kalman gain $\mathbf{K}_k$, thus $\mathbf{K}_k$ is much smaller compare with identity matrix and then causes a rather larger $\mathbf{P}_{k|k}$ after update.
case 3: process noise σ_w^2 have same level as observation noise σ_v^2 shown as the scenario for three position and velocity estimation curves in Fig 5.6: As expected, KF estimation performance degrades with increasing observation noise shown in Fig 5.6. But the KF almostly converges at same time, which can be seen in the lower subfigure of Fig 5.6.

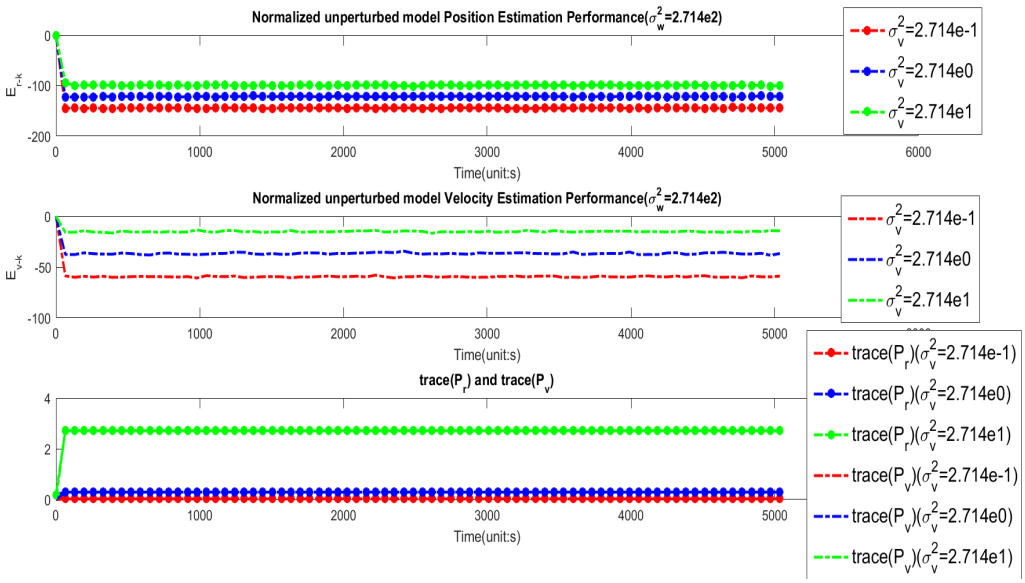

Figure 5.4: Estimation Profile with higher σ_w^2

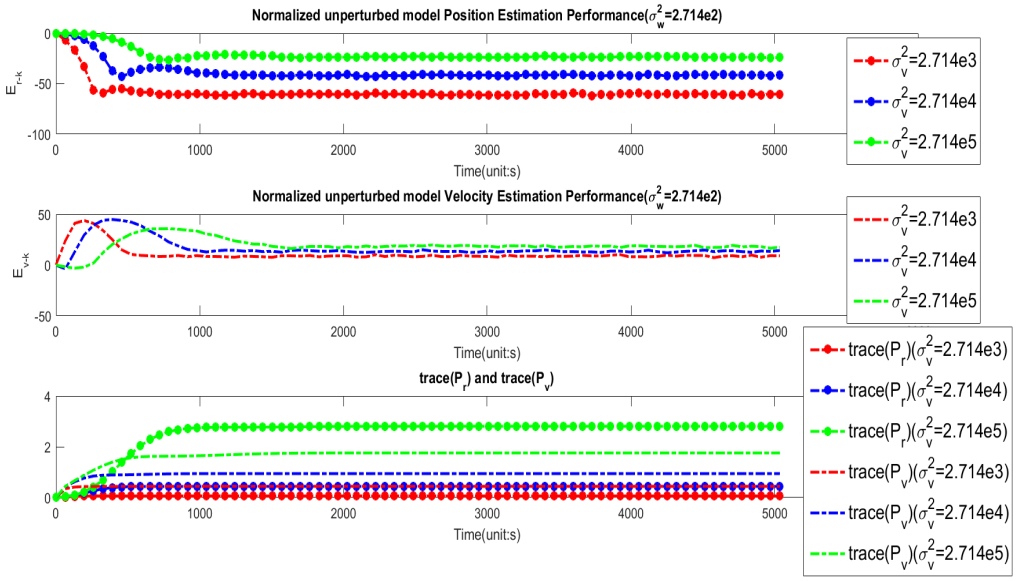

Figure 5.5: Estimation Profile with lower σ_w^2

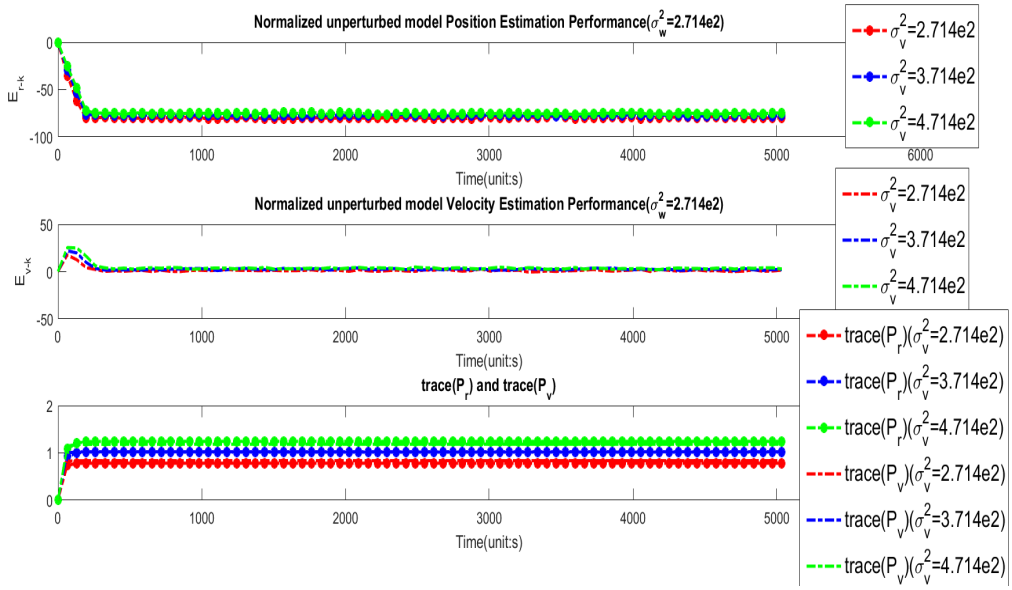

Figure 5.6: Estimation Profile with same level of σ_w^2 and σ_v^2

5.3 Drag-modified and J2-modified HCW model estimation analysis

Drag-modified Model Estimation Results and Analysis

Now we add atmospheric drag force to this approximated projected circular orbit scenario and also generate true state as combination of drag-modified HCW equations plus Gaussian distributed process noise $\mathbf{w}_k$. Estimation profile is shown in Fig 5.7. The initialization of KF is same as in previous section except for increasing observation noise variance range, because overall inter-satellite distance is elevated greatly due to drag force shown in Fig 5.8. To get meaningful estimation error and also consider real scenario, observation noise should increase correspondingly, otherwise, estimation error will be negligible and the whole process can be regarded as noiseless. Similarly, we reuse two metrics with drag-modified state transition matrix $\mathbf{F}_d$ as:

$$\begin{bmatrix} \mathbf{d_{r-metric}} \\ \mathbf{d_{v-metric}} \end{bmatrix} = [\mathbf{F_d} \underbrace{(\mathbf{x}_{k-1} - \mathbf{x}_{k-1|k-1})}_{\mathbf{e}_{k-1}} + \mathbf{w}_k] \tag{5.19}$$

Similarly, the variation in true position and vector magnitude shown in Fig 5.9 influences final estimation error, which also follow calculus of (5.13)-(5.14). The a posterior estimation error in velocity and position portions firstly show a fluctuating increase-decreasing pattern and then converge, which corresponds to residual norm variations in lower sub-figure of Fig 5.8. The variation of normalized position and velocity estimation error in steady state shown in Fig 5.7 is caused by variation of true position and velocity vector norm $||\mathbf{r}_k||$ and $||\mathbf{v}_k||$ in Fig 5.9.

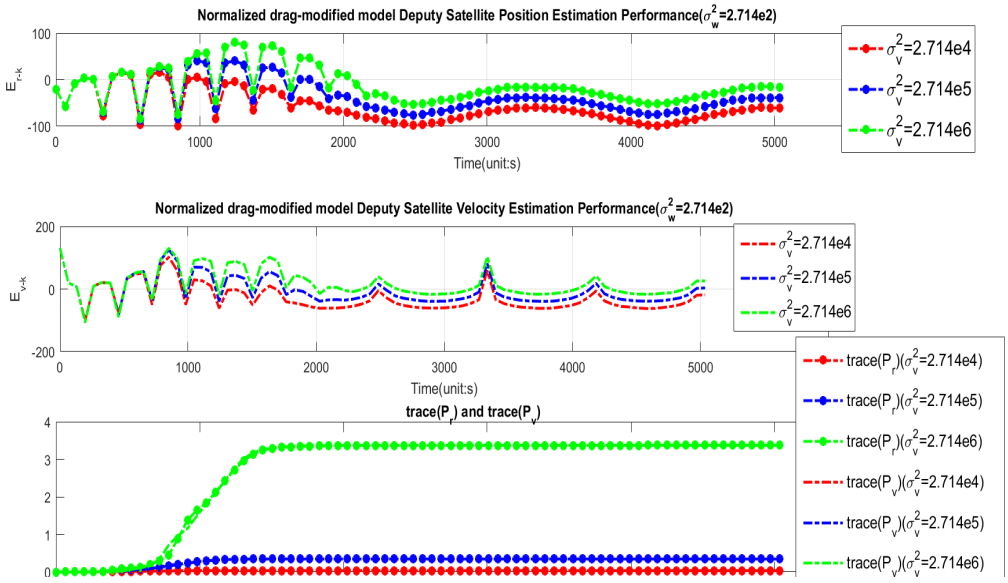

Figure 5.7: Estimation Performance Profile under Atmospheric Drag Force

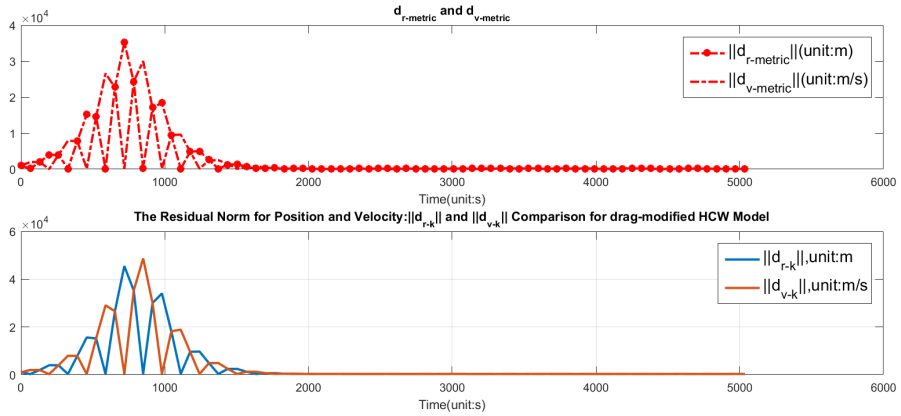

Figure 5.8: Residual Illustration for Drag-modified HCW Model

J2-modified Model Estimation Results and Analysis

Similarly, deputy satellite motion true state in an approximated projected circular orbit with J2 perturbation is calculated as follows:

$$\mathbf{x}_{k+1} = \underbrace{(\Delta t \mathbf{F}_{HCW} + \mathbf{I}_{6\times 6})\mathbf{x}_k + \Delta t \mathbf{u}_{J2}}_{\mathbf{f}_{J2}(\mathbf{x}_k)} + \mathbf{w}_k \tag{5.20}$$

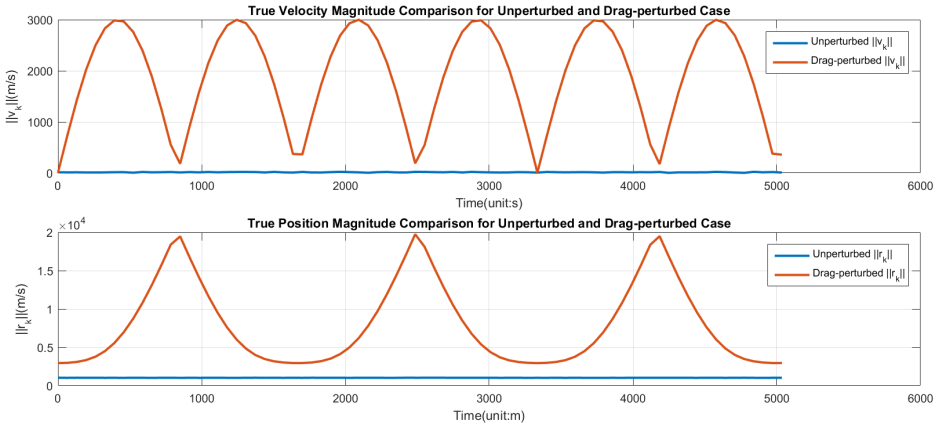

Figure 5.9: True Position and Velocity Magnitude for Drag-modified HCW Model

The process noise variance and observation noise variance are set as $\sigma_w^2 = 2.714e3$ and $\sigma_m^2 = [2.714e2 - 4.714e2]$ for simulation. The reason for choosing a large process noise is to make predict position and velocity estimation error varies steadily. This can be seen in Fig 5.10 that shows decreasing process noise under a fixed observation noise make the velocity and position portion of trace of predict error covariance $trace(\mathbf{P}_r)$ and $trace(\mathbf{P}_v)$ fluctuated more dramatically. The observation noise is also set as large values with consideration of true state position and velocity norm when we include J2 perturbation shown in Fig 5.13. Thus, a small observation noise means our measurement is very good and thus estimation can be regarded as noiseless. The estimation profile is plotted in Fig 5.11.

To analysis steady state error pattern, residual can be rewritten with nonlinear time-varying state transition function $f_{J2-r}(\mathbf{x}_{k|k})$ and $f_{J2-r}(\mathbf{x}_{k|k})$ and are given as:

$$||\mathbf{d}_r|| = ||\mathbf{r_k} + \mathbf{m}_{k-r} - f_{J2-r}(\mathbf{x}_{k|k})|| \tag{5.21}$$

$$||\mathbf{d}_v|| = ||\mathbf{v_k} + \mathbf{m}_{k-v} - f_{J2-v}(\mathbf{x}_{k|k})|| \tag{5.22}$$

where $f_{J2-r}(\mathbf{x}_{k|k})$ is spilt into position and velocity portion as $f_{J2}(\mathbf{x}_{k|k}) = [f_{J2-r}(\mathbf{x}_{k|k}) \quad f_{J2-v}(\mathbf{x}_{k|k})]^T$, $\mathbf{m}_{k-v}$ and $\mathbf{m}_{k-r}$ are observation noises for velocity and position portions. Also, from these residual expression we discover that estimation error at time step $k-1$, observation noise and nonlinear system function at $\mathbf{x}_{k|k}$ will directly influence residual at next time step, and further changes estimation error at next time step and iterate this process. The state transition matrix at given time step is just a linear approximation to the true nonlinear dynamic model, which may cause difference in residual norm $||\mathbf{d}_k||$ even though after KF converges. The Fig 5.13 shows residual for both position and velocity portions increase over time, which implies estimated observation from nonlinear function $f_{J2}(\mathbf{x}_{k|k})$ is less and less to describe true state of deputy satellite under J2 perturbation. As the position and velocity estimation error also follow (5.13)-(5.14), variation in residual and true state in position and velocity part influence estimation error and produce a steady position and velocity error pattern shown in Fig 5.11. The true position and velocity magnitude variation over time is given in fig 5.13. The chief satellite is always closer to Earth than deputy satellite. This can be seen in lower subfigure of Fig 5.14, where orbital height of

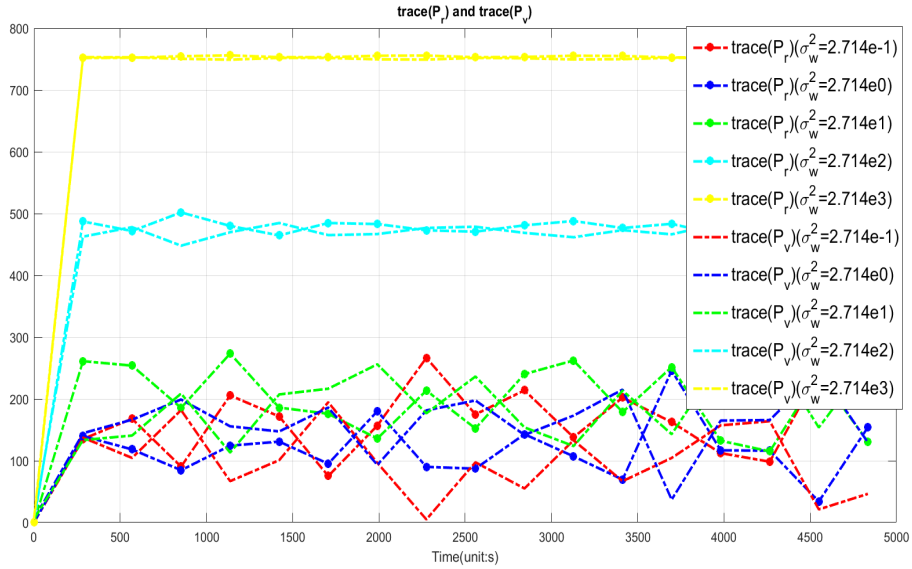

Figure 5.10: $trace(\mathbf{P}_r)$ and $trace(\mathbf{P}_v)$ with Different Process noise($\sigma_v^2 = 2.714e2$)

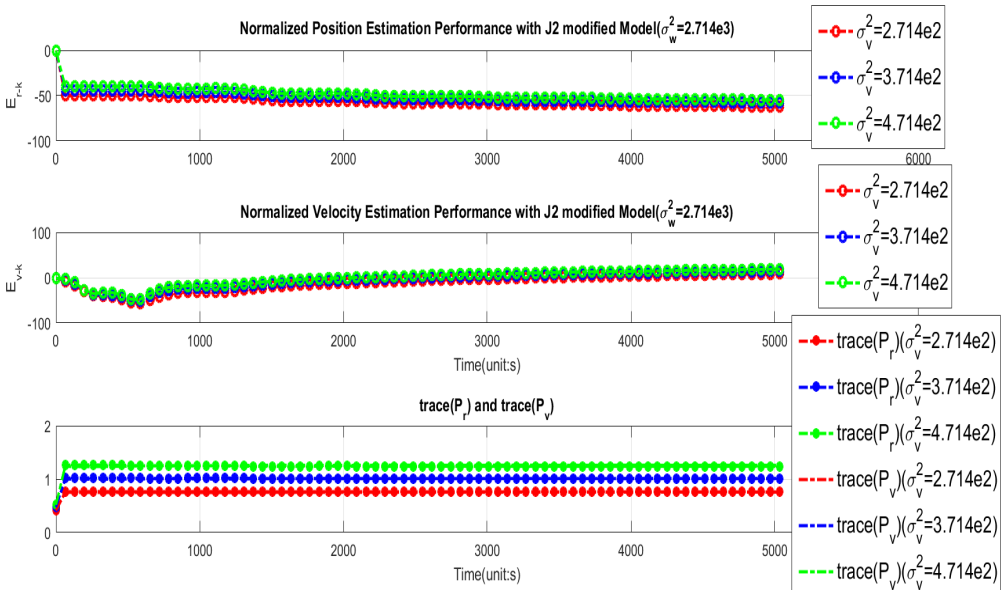

Figure 5.11: EKF Estimation Performance under J2 Perturbation

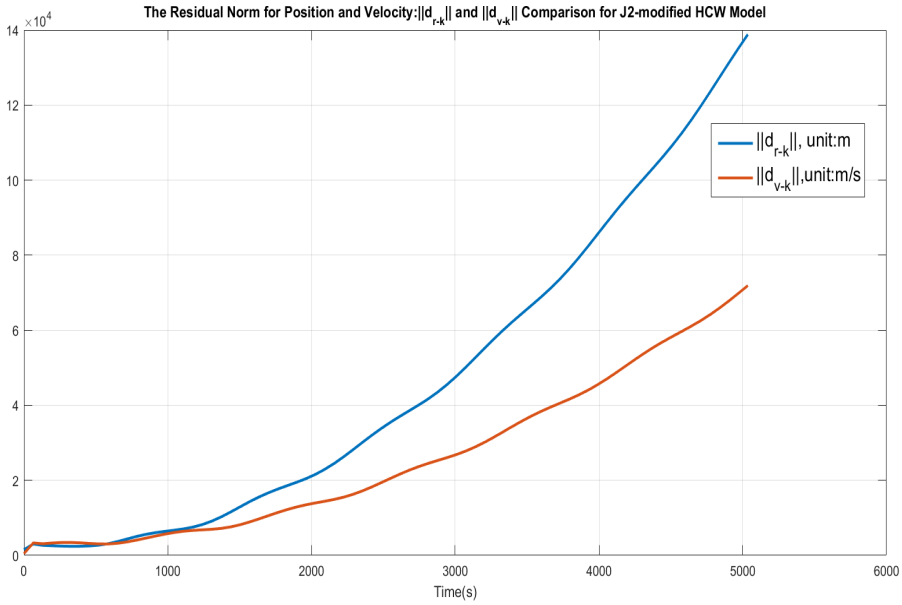

Figure 5.12: Averaged Residual Norm Variation for Position and Velocity Portion

deputy satellite is always larger than the chief one in this approximated PCO. Additionally, we visualize Deputy satellite motion for three cases: unperturbed case, with atmospheric drag force and with J2 perturbation in ECI frame and LVLH frame in Fig 5.14. By comparison its motion in different cases in Fig 5.14, we find out drag force decreases Semi-major axis of original deputy satellite orbit but maintain an ellipitical shape. Satellites in LEO will reduce moving velocity as drag force has anti-parallel direction with respect to their velocity and decreasing velocity results in decrease in Semi-major axis from (2.9). Therefore atmospheric drag force causes orbit decay and results decrease in orbital height and ultimately cause a periodic sine-like and much larger relative distance than unperturbed case shown in Fig 5.9. The J2 perturbation drifts satellite away in x-direction over time, as satellite moves away from Earth means smaller J2 perturbation effect and thus it would move further away due to insufficient gravitational attraction to maintain a bounded motion, thereby causing an increasing inter-satellite distance over time shown in Fig 5.13.

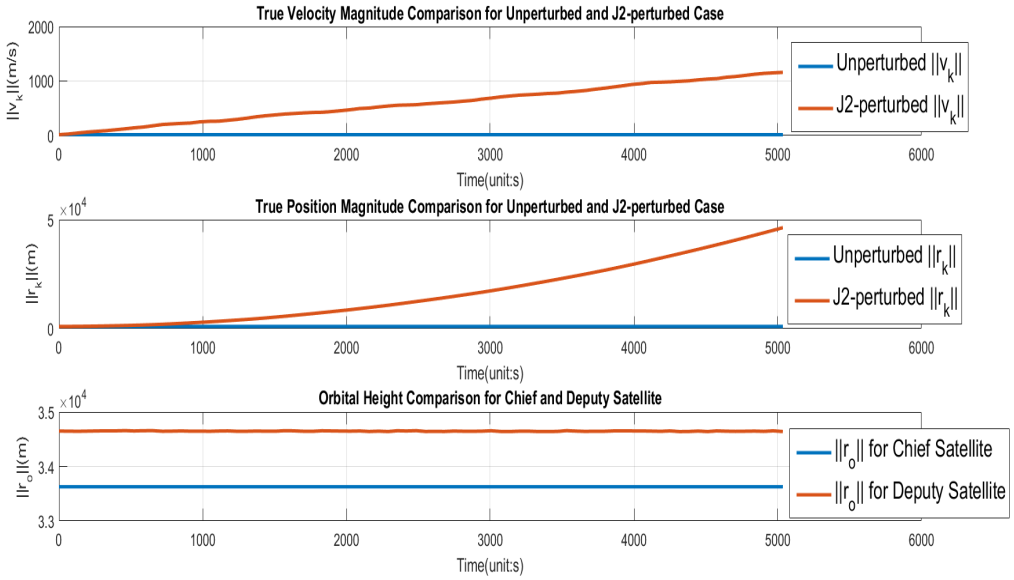

Figure 5.13: Position and Velocity Vector Magnitude:||**r**|| and ||**v**|| Comparison with and without J2

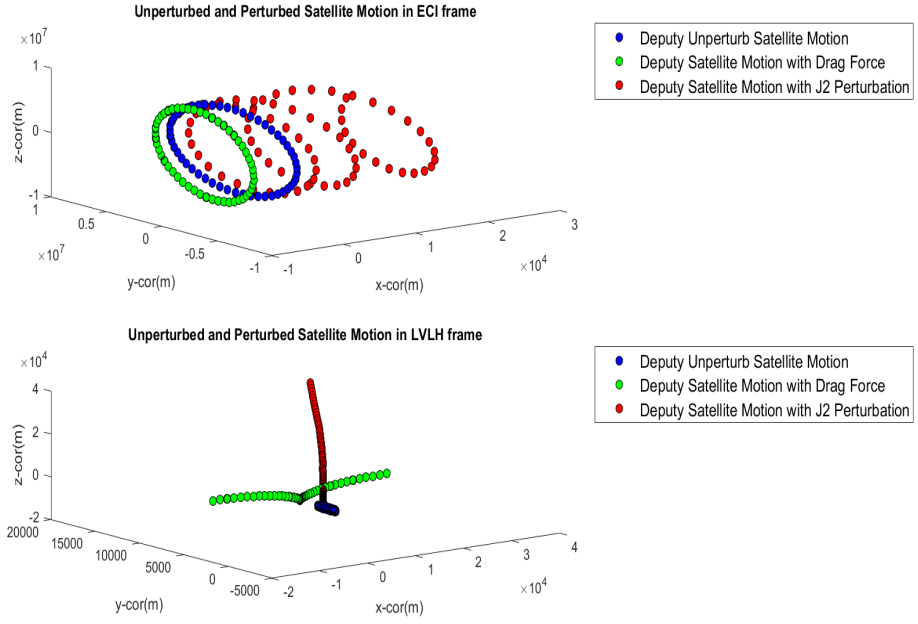

Figure 5.14: Unperturbed and Perturbed Deputy Satellite Motion

Chapter 6

Conclusion

In this project, the investigations of satellite motion in different frames are done and the specific orbit parameters could be chosen to achieve the circular orbits or low eccentric orbits in LEO in ECI frame. From this, we discover circular orbits maintain the minimum stable velocity for satellite. One rotational matrix is applied to transform ECI coordinates to ECEF coordinates that enable us to visualize satellite motion on Earth surface. Furthermore, the combination of different rotational matrices along different axis make it possible to transform satellite motion in LVLH frame and ECI frame.

The projected and general circular orbits originated from HCW model achieve a bounded satellite formation flying. For a typical deputy-chief satellite network a typical deputy-chief satellite network that one satellite is always closer to earth than other one in unperturbed case, the inclusion of atmospheric drag force into HCW model causes satellite orbit decay and thereby elevate inter-satellite distance in an overall sense and show a periodic sine-like pattern. Meanwhile, J2 perturbation causes inter-satellite distance increasing continuously. In Low Earth Orbit with small orbital height, both perturbation are significant, however, atmospheric drag force influence satellite in a finite range and satellite orbit will still be bounded ellipse but J2 perturbation effect is more significant than atmospheric drag force that results larger inter-satellite separation.
Additionally, the increasing observation noise degrades state estimation via KF performance results. From analysis towards KF convergence, we find the KF convergence depends on relative magnitude of process noise and observation noise levels. With the presence of EKF to deal with nonlinear effects in J2-modified HCW model, the appropriate process noise is chosen to avoid dramatic variation of predict position and velocity error.

Also, from the studies of perturbations and classic satellite motion, the optimized path routing and control according to different space mission demands could be consider and extended as future work based on this project.

Chapter 7

appendix

The detailed derivation of HCW equation solution
HCW equations:

$$\Delta\ddot{x} = 3n^2\Delta x + 2n\Delta\dot{y} \tag{7.1}$$

$$\Delta\ddot{y} = -2n\Delta\dot{x} \tag{7.2}$$

$$\Delta\ddot{z} = -n^2\Delta z \tag{7.3}$$

Integrate (7.2):

$$\begin{aligned}\Delta\dot{y} &= -2n\int\Delta\dot{x}\\ &= -2n\Delta x + c\end{aligned} \tag{7.4}$$

substitute (7.4) in (7.1):

$$\Delta\ddot{x} = -n^2\Delta x + 2nc \tag{7.5}$$

(7.5) is a second order differential equation which has general solution as:

$$\Delta x(t) = A_x\cos(nt+\beta_x) + c_1 \tag{7.6}$$

substitute (7.6) in (7.2):

$$\Delta\ddot{y} = 2n^2A_x\sin(nt+\beta_x) \tag{7.7}$$

(7.7) has general solution as:

$$\Delta y(t) = -2A_x\sin(nt+\beta_x) + c_3t + c_2 \tag{7.8}$$

, where c_1, c_2 and c_3 are integral constants. Taking (7.5) and (7.8) into (7.1), we get:

$$-n^2A_x\cos(nt+\beta_x) = 3n^2(A_x\cos(nt+\beta_x)+c_1) + 2n(-2A_x\cos(nt+\beta_x)) + c_3) \tag{7.9}$$

Solve it and get:

$$c_3 = -\frac{3}{2}nc_1 \tag{7.10}$$

then, (7.4) could be rewritten as:

$$\Delta\dot{y} = -2n\Delta x(t) + 2n\Delta x_0 + \Delta\dot{y}_0 \tag{7.11}$$

Equivalently, we could directly calculate $\Delta\dot{y}$ from (7.8), then we get a solution of c_1 via the equivalence of this calculation and calculus in (7.11):

$$2n\Delta x_0 + \Delta\dot{y_0} = \frac{n}{2} \tag{7.12}$$

therefore:

$$c_1 = 4\Delta x_0 + \frac{2\dot{y_0}}{n} \tag{7.13}$$

Then from (7.10), we get:

$$c_3 = -3(2n\Delta x_0 + \dot{y_0}) \tag{7.14}$$

Also, take initial condition for (7.8), we can solve c_2 as:

$$c_2 = 2A_x \sin(nt + \beta_x) + \Delta y_0 \tag{7.15}$$

(7.3) is a second order differential equation which has general solution as:

$$\Delta z(t) = A_z \cos(nt + \beta_z) \tag{7.16}$$

In conclusion, solution of HCW equations can be given from above analysis:

$$\Delta x(t) = A_x \cos(nt + \beta_x) + 4\Delta x_0 + \frac{2\dot{\Delta y_0}}{n} \tag{7.17}$$

$$\Delta y(t) = -2A_x \sin(nt + \beta_x) + 2A_x \sin(\beta_x) + \Delta y_0 - 3(2n\Delta x_0 + \dot{\Delta y_0})t \tag{7.18}$$

$$\Delta z(t) = A_z \cos(nt + \beta_z) \tag{7.19}$$

Acronyms

KF Kalman Filter

EKF Extended Kalman Filter

PCO Projected Circular Orbit

GCO General Circular Orbit

ECI Earth-centered Inertia

ECEF Earth-centered,Earth-Fixed

LVLH Local-Horizontal-Local-Vertical

List of Symbols

$\gamma(t)$	true anomaly
$\mathbf{A}$	Ascending Node Vector
$\mathbf{p}$	Perigee Vector
ω	Argument of Perigee
ϕ	Geocentric latitude
ψ	Longitude
ρ	Atmospheric Density
Ω	Longtitude of Ascending Node
θ	Polar Angle
a	Semi-major axis
e	Eccentricity
G_m	Greenwidch Mean Sideral Time
H	Scale Height
i	Inclination Angle
M	Mean anomaly
n	Angular Velocity
q	Eccentric anomaly
V	Gravitational Potential

Bibliography

[0] H. Djojodihardjo, "The Influence of J2 on Formation Flying of Micro-satellites in Low Near Equatorial Orbits," Journal of Advances in Information technology, vol. 5, no. 1, 2014. 2, 17, 30

[1] *Seeber Gunter, Satellite geodesy, 2nd ed. Berlin: Walter de Gruyter, 2003.* 4, 6, 7, 8, 9, 15, 17, 30

[10] inp J. Bik, P. Visser, and O. Jennrich, "Lisa satellite Formation Control," Advances in Space Research, vol. 40, no. 1, pp. 25–34, 2007. . 21

[2] *Rabenkij Viktor Solomonovic and S. V. Tsynkov, A theoretical introduction to numerical analysis, 1st ed. Boca Raton: Chapman Hall/CRC, 2007.* 12

[3] Y.-G. Lee and H. Bang, "Relative State Estimation of Satellite Formation Flying Using Kalman Filter," IFAC Proceedings, vol. 41, no. 2, pp. 2111–2116, Jul. 2008.

[4] D. E. Catlin, Estimation, Control, and the Discrete Kalman Filter. New York: Springer-Verlag, 1989.

[5] G. krieger, i. hajnsek, k. p. papathanassiou, m. younis, and a. moreira, "Interferometric Synthetic Aperture Radar (sar) Missions Employing Formation Flying," Proceedings of IEEE, vol. 98, no. 5, pp. 816–843, 2010. 21

[6] T. carter and M. humi, "Clohessy-Wiltshire Equations Modified to Include Quadratic Drag," Journal of Guidance, Control, and Dynamics, vol. 25, no. 6, pp. 1058–1063, Aug. 2002. 2, 27, 28

[7] Izzo, Dario and Sabatini, Marco and Valente, C, "A new linear model describing formation flying dynamics under j2 effects," in Proceedings of 17th AIDAA, 2004, vol. 9, pp. 22-28.

[8] Chapter 25 Celestial Mechanics. [online]. available: `https://tmg-web.lehman.edu/faculty/anchordoqui/chapter25.pdf`. 2, 5, 6

[9] "(pdf) Kalman and Extended Kalman filters: Concept, Derivation and Properties," researchgate. [online]. available: `https://www.researchgate.net/publication/2888846_Kalman_and_Extended_Kalman_Filters_Concept_Derivation_and_Properties`. [accessed: 05-aug-2020]. ". 24, 25, 29, 31